EVALUATING PHOSPHATIDYLINOSITIDE AS LIPID BIOMARKERS FOR HYPERGLYCEMIA-RELATED TRIPLE-NEGATIVE BREAST CANCER AGGRESSIVENESS.

Aaron Kile

Submitted to the faculty of the University Graduate School
in partial fulfillment of the requirements
for the degree
Master of Science
in the Department of Biochemistry and Molecular Biology
Indiana University

October 2025

Accepted by the Graduate Faculty of Indiana University, in partial fulfillment of the requirements for the degree of Master of Science.

Master's Thesis Committee

Clark Wells, PhD, Chair

Ann Kimble-Hill, PhD

Anthony J. Baucum, PhD

Angela Richardson, PhD

DEDICATION

To my dad, Lebani Calvin Kile, my mom, Tibasaga Lossi, my sisters, Esther and Elizabeth, and my brother, Nathan. You have been a voice of reason, a pillar of support, a source of encouragement, and a joy to come home to. Thank you for loving me, and above all for always praying for me. I love you all.

ACKNOWLEDGEMENT

I want to first thank God for every opportunity I have had in providence leading up to the accomplishment of this degree and a many other miracles along the way.

I want to acknowledge my committee for their support. You have pushed me to be a better scientist, and a confident contributor to the growing body of rigorous research.

I want to personally thank Dr. Kimble-Hill for her support in both my work in the lab, but also in my professional path. Your support has made a difference for me.

I want to also acknowledge the biochemistry department staff and students for their kindness, selflessness and availability to support me and create a great environment to work.

I want to acknowledge my friends who have seen me through the best and worst parts of my professional and personal life and have been an encouragement to me.

Aaron Kile

EVALUATING PHOSPHATIDYLINOSITIDE AS LIPID BIOMARKERS FOR HYPERGLYCEMIA-RELATED TRIPLE-NEGATIVE BREAST CANCER AGGRESSIVENESS.

Triple-negative breast cancer (TNBC) is the most aggressive breast cancer subtype, marked by limited treatment options and poor patient outcomes. Clinical and epidemiological studies suggest that systemic metabolic conditions, particularly high blood glucose associated with Type 2 Diabetes, may worsen TNBC progression. However, there are no current biomarker for detecting TNBC, especially in hyperglycemic patients.

This thesis investigates how elevated glucose levels influence TNBC behavior and whether lipid signaling molecules at the cell membrane, known as phosphatidylinositol lipids (PIs), can serve as biomarkers of disease progression. To address this, we combined functional assays that measure key cancer traits, including cell migration, attachment to the extracellular matrix (ECM), and cell accumulation, with lipidomic analyses of cell membranes under normal and high-glucose conditions.

Our findings demonstrate that hyperglycemia enhances aggressive traits in TNBC cells, promoting increased movement and growth, but no effect on ECM attachment. In parallel, lipid profiling revealed alterations in PI molecules that regulate growth and survival pathways, with differences observed across cell models. These results highlight a direct connection between metabolic stress and cancer progression. By linking systemic metabolic dysregulation to cell signaling in TNBC, this work identifies PI4P, PI(4,5)P_2

and PIP_3 lipids as potential biomarkers and points toward new strategies for risk stratification and therapeutic intervention.

Clark Wells, PhD, Chair

Ann Kimble-Hill, PhD

Anthony J. Baucum, PhD

Angela Richardson, PhD

TABLE OF CONTENTS

LIST OF FIGURES

LIST OF TABLES

LIST OF ABBREVIATIONS

Adenosine Triphosphate (ATP)

Antibody-drug conjugate (ADC)

Atypical ductal hyperplasia (ADH)

Breast cancer susceptibility gene (BRCA)

Breast conserving surgery (BCS)

Cyclin-dependent kinase 4/6 (CDK 4/6)

Dithiothreitol (DTT)

Ductal carcinoma in situ (DCIS)

Enhanced chemiluminescence (ECL)

Epithelium-to-mesenchymal transition (EMT)

Estrogen receptor (ER)

Extracellular matrix (ECM)

Fetal bovine serum (FBS)

Giant plasma membrane vesicle (GPMV)

Hormone receptors (HR)

Human embryonic kidney 293T (HEK293T)

Human epidermal growth factor receptor 2 (HER2)

Immune checkpoint inhibitors (ICIs)

Immunohistochemistry (IHC)

Invasive ductal carcinoma (IDC)

Koman tissue bank (KTB)

Lobular carcinoma in situ (LCIS)

Near infrared 680 (NIR680)

Oxidative phosphorylation (OXPHOS)

Paraformaldehyde (PFA)

Pentose phosphate pathway (PPP)

Phosphatidylinositol (PI)

Phosphoinositide (PIP)

Phosphoinositide 3-kinases (PI3Ks)

Progesterone receptor (PR)

Selective estrogen receptor degrader (SERD)

Selective estrogen receptor modulator (SERM)

Tricarboxylic acid cycle (TCA)

Triple-negative breast cancer (TNBC)

Tumor microenvironment (TME)

Type 2 diabetes (T2D)

Chapter 1 – Introduction and Background

1.1 Breast Cancer Statistics and Clinical Relevance

Breast cancer is the most frequently diagnosed cancer among women worldwide and remains the second leading cause of cancer-related mortality [1]. In the United States, projections for 2025 estimate 316,950 new cases of invasive breast cancer and 42,170 related deaths [2]. Accounting for approximately 32% of all cancer diagnoses in women [2], breast cancer represents a major public health challenge. Its etiology and progression are shaped by a complex interplay of genetic, epigenetic, and environmental factors. Understanding the risk factors that influence breast cancer onset and progression is essential for improving patient outcomes, particularly in aggressive subtypes where therapeutic options remain limited.

1.2 Breast Tissue Architecture

Normal breast tissue is composed primarily of adipose and glandular elements. Without skeletal support, the breast is anchored to the chest wall by ligaments, resting on the pectoralis major, with boundaries extending from the sternum to the axilla and the latissimus dorsi [3]. Architecturally, the breast is organized into lobes and lobules connected by a ductal system and surrounded by a matrix of adipose, connective, and vascular tissues [4], [5]. Beyond its role in lactation and infant nourishment, the breast also plays a regulatory role in endocrine signaling, influencing processes such as the menstrual cycle, pregnancy, and menopause [6]. Hormones including estrogen, progesterone, and prolactin are central to these processes.

At the imaging level, breast tissue density and organization serve as clinical indicators of abnormal growth and breast cancer risk [7]. At the cellular level, the maintenance of

apical–basal polarity in epithelial cells is essential for lipid and protein organization, cell-to-cell signaling, and adhesion to the extracellular matrix [8]. This polarized architecture enables proper spatial distribution of proteins and lipids, ensuring tissue homeostasis and signaling fidelity.

1.3 Pathogenesis of Breast Cancer

Disruption of tissue polarity often marks the earliest transition from healthy epithelium to neoplastic growth. Loss of polarity in ductal epithelial cells can initiate hyperplasia, progress to atypical ductal hyperplasia (ADH), and evolve into ductal carcinoma in situ (DCIS) [9]. This progression involves both genetic and environmental drivers, leading to histological and molecular alterations. Changes during the transition from normal tissue to DCIS include altered hormonal signaling, autocrine growth factor secretion, and recruitment of inflammatory and stromal cells, which collectively contribute to immune evasion [4]. While DCIS is classified as non-invasive, 25–60% of cases may progress to invasive ductal carcinoma (IDC) [10]. Thus, identifying molecular changes that distinguish indolent from aggressive lesions remains a critical challenge.

One hallmark of breast cancer progression from DCIS to IDC is the breakdown of epithelial architecture at primary disease sites. This process triggers abnormal proliferation, cytokine-mediated signaling, dedifferentiation, and asymmetric protein and lipid localization, reinforcing oncogenic signaling loops [8]. These changes are frequently accompanied by epithelial–mesenchymal transition (EMT), particularly at the tumor–stroma interface [8], [11], [12]. Such structural and molecular alterations are pivotal for metastatic spread, underscoring the importance of understanding risk factors and polarity-disrupting events that drive breast cancer aggressiveness.

1.4 Breast Cancer Subtypes and Treatment Options

Histopathology has long served as the basis for breast cancer classification; however, molecular profiling has refined tumor categorization into luminal A, luminal B, HER2-positive, and basal-like subtypes, distinguished by gene expression profiles [13]. Immunohistochemistry (IHC) for hormone receptors, estrogen receptor (ER), progesterone receptor (PR), and human epidermal growth factor receptor 2 (HER2), further stratifies tumors into clinically actionable groups: hormone receptor-positive (HR+), HER2+, and triple-negative breast cancer (TNBC) [14]. These subtypes guide therapeutic decisions and prognostic expectations. HR+ and HER2+ tumors benefit from targeted therapies, while TNBC remains the most aggressive and least responsive to current treatment strategies.

1.5 Therapeutic Advances and Gaps in TNBC

Over the past decade, advances in molecular diagnostics have improved early detection and informed precision therapies, particularly in HR+ and HER2+ subtypes [15]. Surgical management has also shifted toward less invasive approaches, with breast-conserving surgeries (BCS) increasingly favored over radical mastectomies [16]. Thermal ablation and cryoablation represent additional minimally invasive options [15].

For HR+ breast cancer, selective estrogen receptor modulators (SERMs), selective estrogen receptor degraders (SERDs), and aromatase inhibitors form the foundation of endocrine therapy, often in combination with cyclin-dependent kinase 4/6 (CDK4/6) inhibitors [17], [18]. More recently, inhibitors targeting the PI3K/AKT/mTOR pathway have shown promise, particularly in overcoming endocrine resistance [19]. Immune

checkpoint inhibitors (ICIs) have also demonstrated efficacy when combined with endocrine therapy, further improving outcomes [20], [21].

HER2+ breast cancer has benefited significantly from targeted therapies. Standard treatment includes monoclonal antibodies trastuzumab and pertuzumab, typically administered with chemotherapy [15]. Antibody–drug conjugates (ADCs) have emerged as powerful tools, coupling targeted antibodies to cytotoxic payloads, thereby improving drug delivery and minimizing systemic toxicity [22], [23]. Research into HER2-directed vaccines and approaches addressing HER2 heterogeneity continues to expand therapeutic options [24].

In contrast, TNBC lacks established targeted therapies due to absent ER, PR, and HER2 expression [15]. Although therapies targeting BRCA mutations, Trop-2, and immune checkpoints have shown potential, their efficacy remains limited to select patient subsets [25], [26], [27], [28]. Notably, dysregulation of the PI3K/AKT/mTOR pathway is common in TNBC, contributing to multidrug resistance and metastatic progression [29], [30]. Addressing this gap requires the development of biomarkers that can stratify risk and guide targeted therapy in TNBC.

1.6 Breast Cancer Risk Factors and Their Role in TNBC Aggressiveness

Alongside hereditary predispositions (e.g., BRCA1/2 mutations), metabolic and lifestyle factors such as obesity, alcohol consumption, and type 2 diabetes (T2D) are increasingly recognized as key drivers of breast cancer risk [31]. TNBC, in particular, demonstrates profound metabolic reprogramming, enabling tumor cells to meet the energetic and biosynthetic demands of rapid proliferation [32].

T2D is characterized by chronic hyperglycemia and insulin resistance, both of which activate oncogenic pathways [33]. Persistent hyperglycemia alters cellular signaling and has been associated with increased breast cancer incidence and mortality [34], [35], particularly among women with TNBC [36]. While the relationship between T2D-related hyperglycemia and breast cancer progression has been studied extensively, translational work is needed to identify predictive biomarkers of hyperglycemia-driven TNBC aggressiveness.

1.7 Glucose Metabolism and the Warburg Effect in Cancer

Glucose metabolism is central to the link between T2D and breast cancer risk. Under physiological conditions, glucose is metabolized via glycolysis and oxidative phosphorylation (OXPHOS) to efficiently generate ATP [37], [38]. Cancer cells, however, preferentially engage aerobic glycolysis, a phenomenon termed the Warburg effect [39]. In this metabolic program, glycolysis provides ATP while diverting carbon intermediates into biosynthetic pathways for nucleotides, lipids, and proteins [40], [41]. This shift promotes rapid growth and generates lactate, which acidifies the tumor microenvironment (TME), facilitating immune evasion and pro-migratory signaling via PI3K/AKT/CREB pathways [42], [43].

Thus, the Warburg effect not only supports energy demands but also remodels signaling networks and the extracellular milieu, promoting aggressive tumor phenotypes. The PI3K pathway, in particular, plays a critical role in integrating these metabolic and signaling cues.

1.8 PI3K: A Molecular Nexus Linking Metabolism and TNBC Progression

The PI3K signaling pathway is central to regulating cell growth, metabolism, angiogenesis, survival, and motility [44]. Activated class I PI3Ks phosphorylate phosphatidylinositol 4,5-bisphosphate ($PI(4,5)P_2$), generating phosphatidylinositol 3,4,5-trisphosphate ($PI(3,4,5)P_3$). This lipid recruits pleckstrin homology (PH)-domain proteins such as AKT and PDK1 to the plasma membrane, initiating downstream oncogenic signaling [44]. PI3K/AKT signaling regulates cytoskeletal organization, DNA repair, apoptosis resistance, glucose metabolism, and protein translation [45].

Mutations in PIK3CA and loss of the phosphatase PTEN are common in breast cancer, particularly TNBC, leading to sustained PI3K/AKT/mTOR activation. This drives glycolytic metabolism, EMT, and multidrug resistance [46]. Thus, PI lipid signaling represents a mechanistic crossroads linking metabolic dysregulation to TNBC aggressiveness.

1.9 Phosphatidylinositol Lipids: Signaling Mediators

Phosphorylated derivatives of phosphatidylinositol (PIs), collectively termed phosphoinositide (PIPs), are essential signaling molecules [47]. Their phosphorylation at the 3', 4', and/or 5' positions of the inositol ring produce derivatives with distinct spatial and temporal roles in cellular signaling and trafficking [48], [49], [50]. These include PI(3)P, PI(4)P, $PI(3,4)P_2$, $PI(3,5)P_2$, $PI(4,5)P_2$, and $PI(3,4,5)P_3$ (PIP3). Differential enrichment of PIPs at organelle membranes confers membrane identity and directs processes such as cytoskeletal dynamics, endocytosis, exocytosis, vesicular trafficking, etc. [48], [51].

Of particular relevance, $PI(4,5)P_2$, enriched at the plasma membrane, serves as the primary substrate for PI3K. Its phosphorylation to $PI(3,4,5)P_3$ initiates lipid-mediated signal transduction by recruiting AKT and related proteins [52], [53]. $PI(3,4)P_2$, once considered only a PIP3 degradation product, is now recognized as a distinct signaling entity involved in cytoskeletal remodeling, clathrin-mediated endocytosis, and mTOR regulation [54]. Kinases (e.g., class I/II PI3Ks) and phosphatases (e.g., PTEN, SHIP) tightly regulate these transitions to maintain spatiotemporal signaling fidelity [47].

1.10 PI Dysregulation and Biomarker Potential in TNBC

PI metabolism is frequently dysregulated in cancer. PI kinases and phosphatases are among the most commonly mutated proteins in aggressive breast cancer [52]. Hyperactivation of the PI3K/AKT pathway, often through accumulation of $PI(3,4,5)P_3$, promotes survival, proliferation, EMT, and metastasis [53]. Dysregulated PIP signaling also alters cytoskeletal organization and cell adhesion, further contributing to invasive phenotypes [53].

Recent studies demonstrate that T2D-associated hyperglycemia significantly alters the plasma membrane lipidome across HR+, HER2+, and TNBC cell lines [55]. These findings suggest that hyperglycemic stress reprograms phospholipid signaling and may contribute to breast cancer aggressiveness.

The present study aims to build on this knowledge by characterizing PI signaling under hyperglycemic stress in aggressive TNBC. Specifically, this work surveys breast cancer and non-breast cancer cell lines under hyperglycemia, employing functional assays of aggressive phenotypes and antibody-based detection of PI derivatives. By characterizing the abundance and phosphorylation states of PI lipids in TNBC, this study seeks to

identify novel lipidomic biomarkers and elucidate mechanistic links between metabolic disease and cancer progression.

Chapter 2 – Materials and Methods

2.1 Cell Lines and Reagents

Human embryonic kidney 293T (HEK293T) cells were obtained from Dr. Clark Wells (Indiana University School of Medicine, Indianapolis, IN, USA), and Komen Tissue Bank 36 (KTB36), an epithelial normal breast cell line was obtained from Dr. Harikrishna Nakshatri (Indiana University School of Medicine, Indianapolis, IN, USA). Triple-negative breast cancer (TNBC) cell lines included HCC38 epithelial cells, originally isolated from the mammary gland of a post-menopausal female with stage IIB, grade 3 ductal carcinoma; HCC1806 epithelial cells, derived from the mammary gland of a post-menopausal female with stage IIB, grade 2 acantholytic squamous cell carcinoma; HS578T epithelial cells, isolated from the breast tissue of a post-menopausal woman with ductal carcinoma; MDA-MB-468 epithelial cells, derived from a pleural effusion of a post-menopausal woman with metastatic breast adenocarcinoma; and MDA-MB-231 epithelial cells, also derived from a pleural effusion of a post-menopausal woman with metastatic mammary adenocarcinoma. All TNBC cell lines were purchased from the American Type Culture Collection (ATCC, Manassas, VA, USA).

Cells were cultured in Dulbecco's Modified Eagle Medium (DMEM; Corning, Manassas, VA, USA) supplemented with either 1 g/L (normal glucose) or 4.5 g/L (hyperglycemic) D-glucose, 2 mM L-glutamine, 1 mM sodium pyruvate, 10% fetal bovine serum (FBS; Peak Serum, Denver, CO, USA), and 1% penicillin–streptomycin. Primary mouse antibodies specific for phosphatidylinositol species were obtained from Echelon Biosciences (Salt Lake City, UT, USA), including antibodies against PI3P (Z-P003), PI4P (Z-P004), $PI(3,4)P_2$ (Z-P034b), $PI(3,5)P_2$ (Z-P035), $PI(4,5)P_2$ (Z-P045), and PIP_3

(Z-P345). Fluorescent secondary antibodies included Alexa Fluor 680 goat anti-mouse IgG (A21057), Alexa Fluor 790 goat anti-mouse IgG (A11375), Qdot 525 goat $F(ab')_2$ anti-mouse IgG (Q11041MP), and AF488-conjugated goat anti-mouse IgG (Jackson ImmunoResearch, Cat. No. 1031-30). Collagen-coated plates were obtained from Greiner Bio-One (North Carolina, USA), and fibronectin-coated PureCoat™ plates were purchased from Corning (Manassas, VA, USA). Amersham Protran 0.2 μm nitrocellulose membranes were sourced from Cytiva (Wilmington, DE, USA). BioTracker NIR680 cytoplasmic membrane dye was purchased from EMD Millipore (Darmstadt, Germany), and the CellTiter 96® AQueous One Solution Cell Proliferation Assay was obtained from Promega (Madison, WI, USA). Fluorescence imaging was performed using either the EVOS M5000 imaging system (Thermo Fisher Scientific, Indianapolis, IN, USA) or the LI-COR Odyssey Imaging system (LI-COR Biosciences, Lincoln, NE, USA).

2.2 Methods

2.2.1 Transwell Migration Assay

Cell migration was assessed using Nunc polycarbonate trans-well inserts (Thermo Fisher Scientific) in 24-well format. A total of 1×10^5 cells, conditioned in either normal glucose or hyperglycemic media, were seeded into the upper chamber. The lower chamber was filled with 200 μL of complete DMEM supplemented with either normal or elevated glucose as a chemoattractant. Following a 24-hour incubation at 37 °C, migrated cells in the lower chamber were quantified using the CellTiter 96® reagent, and absorbance was measured at 490 nm. Migration efficiency was expressed relative to control wells in which cells were directly seeded into the lower chamber (positive control), and percent migration was calculated as

$$\%\ Migration = \frac{Absorbance\ of\ Migrated\ Cells}{Absorbance\ of\ Positive\ Control} X\ 100$$

2.2.2 Scratch (Wound-Healing) Assay

For the scratch (wound-healing) assay, cells were seeded into 6-well or 24-well plates and grown to confluency. Wounds were created using a sterile pipette tip (P2 for 6-well and P20 for 24-well plates). Guide marks were drawn on the underside of the plates to ensure consistent imaging. Wound closure was monitored over 24 hours and imaged using the EVOS M5000 microscope. Quantification was performed with the Wound Healing plugin in Fiji/ImageJ, and closure was expressed as the percentage reduction in wound area at 24 hours relative to the initial wound size according to the formula:

$$\%\ Wound\ Closure = \frac{(Area\ at\ time\ 0 - Area\ at\ 24\ hours)}{Area\ at\ time\ 0} X\ 100$$

2.2.3 Cell Attachment Assay

For the cell attachment assays, cells were pre-labeled with the NIR680 dye (1:20,000 dilution in respective glucose-conditioned media) for 1 hour and plated onto collagen- or fibronectin-coated plates in DMEM supplemented with 10% FBS under either normal glucose or hyperglycemic conditions. Adhesion was assessed at 30 minutes and at 16 hours (representing maximum attachment). At each time point, wells were washed with PBS and fluorescence was quantified using the LI-COR Odyssey. Percent attachment was calculated as:

$$\%\ Attachemt\ in\ 30\ mins = \frac{Intensity\ at\ 30\ mins}{Intensity\ at\ 16\ hours} X\ 100$$

2.2.4 Cell Accumulation Assay

Cell accumulation assays were performed by pre-labeling cells overnight with NIR680 in either normal glucose or hyperglycemic DMEM. The following day, 55 µL or 100 µL of cells were seeded into 96-well plates and allowed to adhere for 1 hour prior to baseline imaging (Day 0). Fluorescence imaging was conducted daily for four to five days using the LI-COR Odyssey. On Days four and five, additional NIR680 was added to label newly synthesized membranes of proliferating cells. Fluorescence intensities were quantified with Fiji/ImageJ and normalized to Day 0 values using the equation N(t)/N(0), where N(t) is the fluorescence intensity on any given day.

2.2.5 Isolation of Giant Plasma Membrane Vesicles (GPMVs)

To isolate giant plasma membrane vesicles (GPMVs), confluent cells in 100 mm dishes were washed with GPMV buffer (10 mM HEPES, 150 mM NaCl, 2 mM $CaCl_2$, pH 7.4) and incubated in buffer containing 25 mM paraformaldehyde and 2 mM dithiothreitol for 1 hour at 37 °C. The supernatant containing vesicles was collected, centrifuged at 1,500 × g for 2 minutes to remove debris, and either used immediately in spot blot assays or stored at –80 °C.

2.2.6 Phosphatidylinositol Detection via Spot Blot Assay

Phosphatidylinositol detection by spot blot assay was performed by spotting 2 µL of GPMV lysates onto Amersham Enhanced Chemiluminescence (ECL) membranes pre-gridded using a 96-well template. After air drying, membranes were blocked with 1% non-fat milk in PBST (PBS + 0.1% Tween-20) for 30 minutes. Primary antibodies against phosphatidylinositol species (1:1000) were pre-incubated with their respective fluorescently labeled secondary antibodies (1:2000) for 30 minutes at room temperature

before application to the membranes. Antibody–fluorophore pairs were as follows: PI3P with Alexa Fluor 790 (imaged at 800 nm); PI4P and PI(3,5)P_2 with AF488 (imaged at 488 nm); PI(3,4)P_2 and PI(4,5)P_2 with Qdot 525 (imaged at 520 nm); and PIP_3 with Alexa Fluor 680 (imaged at 700 nm). Following incubation, membranes were washed three times with PBST and imaged with the LI-COR Odyssey. Signal intensities were quantified using Fiji/ImageJ.

2.2.7 High-Throughput Biomarker Screen of Cellular Phosphatidylinositol

For the high-throughput biomarker screen of phosphatidylinositol species, cells were seeded in 96-well plates (25 µL per well) and cultured in either normal glucose or hyperglycemic DMEM. Antibodies were tested in technical triplicates. After NIR680 labeling and baseline imaging, cells were incubated for 1 hour with antibody mixtures consisting of a mouse anti-phosphatidylinositol primary antibody and an anti-mouse Alexa Fluor 790-conjugated secondary antibody. Wells were washed twice with PBS and imaged at 700 nm (NIR680 signal) and 800 nm (phosphoinositide antibody signal). Signal intensity was expressed as a percentage using the formula:

$$\%\ PIP\ Bound = \frac{PI\ antibody\ signal\ intensity}{NIR680\ signal\ intesntiy} X\ 100$$

2.3 Data Acquisition and Analysis

Image data acquired from EVOS and LI-COR systems were exported as TIFF files and analyzed in Fiji/ImageJ, with background correction applied prior to quantification. Statistical analyses were performed in Microsoft Excel, and graphs were generated in JMP (SAS Institute). Comparisons between groups were assessed using two-tailed unpaired Student's t-tests unless otherwise noted, with significance defined as $p < 0.05$.

All experiments were independently repeated in at least three biological replicates unless otherwise specified.

Chapter 3 – Results

3.1 Functional Measures of Hyperglycemia-Dependent Breast Cancer Aggressive Phenotypes

The objective of this study was to evaluate how hyperglycemia influences aggressive breast cancer phenotypes by comparing triple-negative breast cancer (TNBC) cell lines across a set of orthogonal functional assays. Specifically, we assessed cell migration, extracellular matrix (ECM) attachment and proliferation under normal glucose and hyperglycemic conditions. These assays provide complementary perspectives on how glucose availability may drive tumor cell aggressiveness by modulating motility, attachment and growth dynamics, aspects that play a role in breast cancer aggressive phenotypes.

To further explore the biomarker potential of phosphatidylinositol (PI) lipids in these processes, we conducted two additional assays: a giant plasma membrane vesicle (GPMV) assay to quantify the accumulation of PI derivatives at the plasma membrane, and a live-cell antibody binding assay to evaluate surface accessibility of PI lipids under varying glucose conditions.

3.1.1 Transwell Migration – Glucose-Driven Chemotaxis

We first evaluated glucose-driven chemotaxis using a trans-well migration assay, in which cells migrate through a porous membrane toward media containing either normal or high glucose as the chemoattractant. This assay provides a quantitative measure of the intrinsic migratory capacity of cells in response to glucose gradients, offering insight into how metabolic cues shape tumor cell behavior. Since hyperglycemia is known to enhance tumor aggressiveness and promote metastatic dissemination, we hypothesized that all

TNBC cell lines would exhibit preferential migration toward hyperglycemic media. By directly comparing migration under normal glucose versus hyperglycemic conditions, this assay allowed us to test whether elevated glucose availability functions as a chemoattractant that drives TNBC motility.

Consistent with our hypothesis, HCC1806 cells exhibited a significant increase in migration, approximately 10% higher toward hyperglycemic media compared to normal glucose conditions (Fig. 1A). HCC1806 TNBC cells may directly exploit elevated glucose availability as a chemoattractant to enhance motility. In contrast, HCC38 and Hs578T cells showed no significant differences in migration between glucose conditions, although HCC38 displayed a slight but non-significant trend toward reduced migration in hyperglycemia (Fig. 1B–C). Interestingly, MDA-MB-231 cells responded in the opposite manner, with migration decreasing by roughly 15% under hyperglycemic conditions (Fig. 1D). This unexpected reduction highlights potential heterogeneity in glucose sensitivity across TNBC cell lines, suggesting that distinct metabolic adaptations or signaling networks may dictate whether hyperglycemia promotes or suppresses motility.

Fig. 1

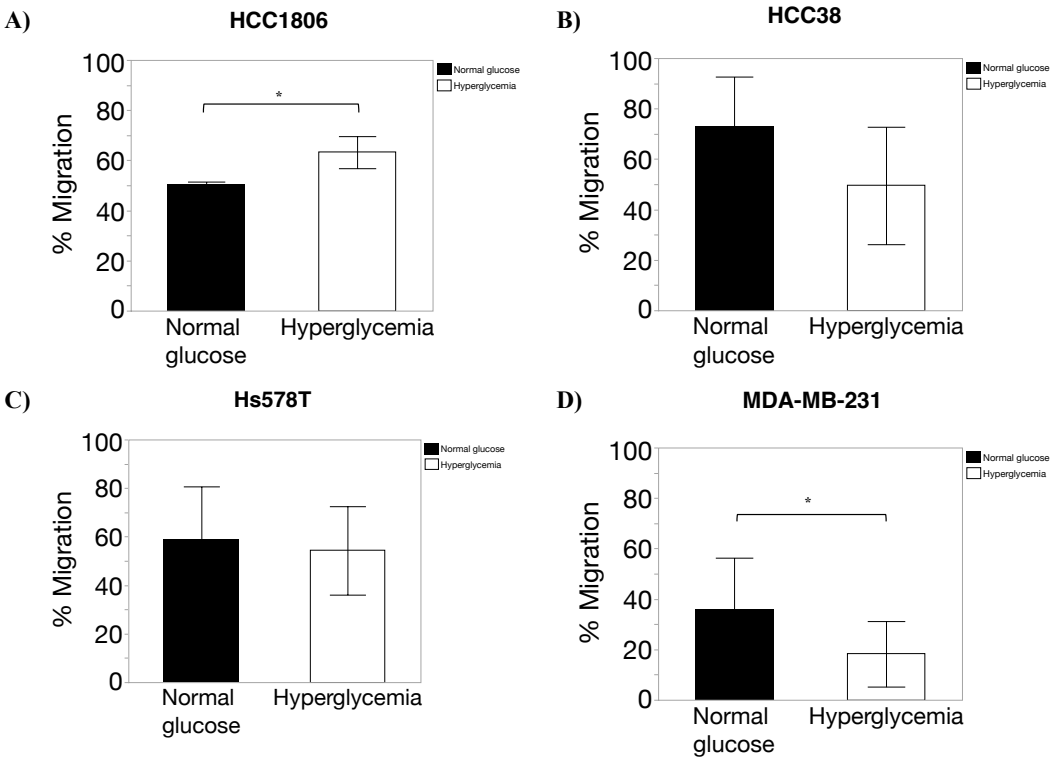

Figure 1 | Effect of Hyperglycemia on Transwell Migration in Aggressive TNBC Cell Lines. Bar graphs depict overnight trans-well migration of (A) HCC1806 (normoglycemia, $n = 3$; hyperglycemia, $n = 3$), (B) HCC38 ($n = 3$; $n = 8$), (C) Hs578T ($n = 5$; $n = 6$), and (D) MDA-MB-231 ($n = 14$; $n = 9$) cells under normoglycemic or hyperglycemic conditions. Bars represent mean values, and error bars indicate ± s.d., calculated from independent measurements. Statistical significance was determined using unpaired Student's *t*-test with unequal variance; $P < 0.05$

When migration was compared across cell lines, HCC1806 displayed significantly higher trans-well migration than MDA-MB-231 under normal glucose, and under hyperglycemia HCC1806, HCC38, and Hs578T all migrated more efficiently than MDA-MB-231 (Fig. 2). Among all TNBC cell lines tested, MDA-MB-231 consistently demonstrated the lowest migratory capacity across both glucose conditions. This relative insensitivity may

reflect unique genetic or metabolic features of this cell line, such as KRAS mutations or altered PI3K/AKT signaling, which could dampen glucose-driven chemotaxis.

Fig. 2

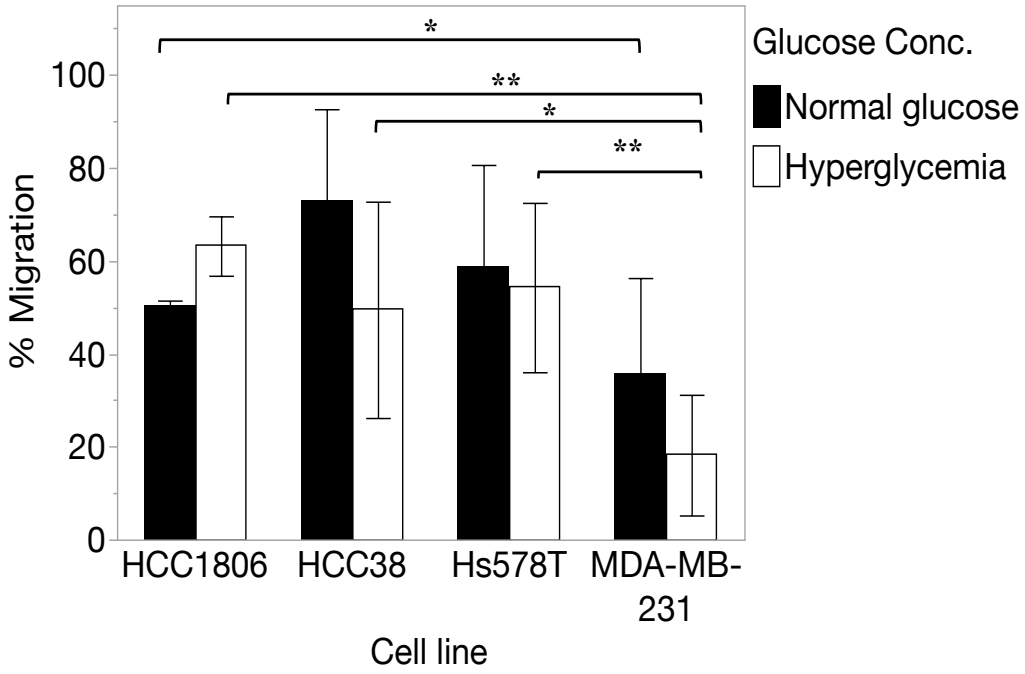

Figure 2 | Transwell Migration of Aggressive TNBC Cell Lines Under Normal and Hyperglycemic Conditions. HCC1806, HCC38, Hs578T, and MDA-MB-231 cells were assessed for migration using a trans-well assay. Bars represent mean values, and error bars indicate ± s.d. from independent measurements. Statistical significance was determined using a two-tailed Student's t-test with unequal variance; *$P < 0.05$, **$P < 0.005$

These results indicate that hyperglycemia does not uniformly enhance chemotaxis across TNBC cell lines. While HCC1806 responded as predicted, MDA-MB-231 demonstrated impaired migration, suggesting cell line–specific metabolic dependencies. While

hyperglycemia broadly enhances migration in some TNBC subtypes, others may exhibit resistance or even suppression, underscoring the complexity of glucose–tumor interactions. Fold differences between the cell lines are shown in table 1 in the appendix.

Some limitations in our approach to the trans-well assay constrain the extent of these experimental observations. Specifically, only cells that migrated to the lower chamber were quantified, while non-migratory cells remaining in the upper chamber were not assessed. Future experiments should account for both populations to better capture migration efficiency relative to seeding density. Moreover, the assay provides only an endpoint measurement, offering no insight into real-time migratory dynamics or the temporal regulation of metastasis-related behavior.

3.1.2 Scratch Wound Closure

To further evaluate cell migration independent of an imposed chemoattractant gradient, we performed a scratch wound assay. Unlike the trans-well migration assay, which quantifies directed cell movement through a porous membrane toward a chemoattractant, the scratch assay measures the collective ability of cells to migrate across a two-dimensional surface to close an artificial wound. This approach provides a dynamic view of migratory behavior, capturing not only the speed and coordination of wound closure but also contributions from cell–cell interactions. Importantly, wound closure reflects a combination of cell migration and proliferation, offering a more physiologically relevant representation of how tumor cells repopulate space after tissue disruption. By comparing wound closure in normal versus hyperglycemic conditions, we hypothesized that TNBC cells would display accelerated closure under hyperglycemia, indicating an enhanced migratory phenotype in the absence of chemotactic cues.

Consistent with our hypothesis, HCC1806 and HCC38 cells demonstrated significantly enhanced wound closure under hyperglycemia, whereas Hs578T, MDA-MB-231, and MDA-MB-468 showed no significant differences between glucose conditions (Fig. 3A–E). HCC1806 recapitulated the trend observed in the trans-well assay, exhibiting a hyperglycemia-dependent increase in migratory behavior across both assays. In contrast, HCC38 displayed divergent behavior between assays: while trans-well migration showed no significant change (with a slight trend favoring normal glucose), wound closure was significantly accelerated under hyperglycemia. Hs578T cells remained unresponsive in both assays, suggesting that their migratory phenotype is not strongly modulated by glucose availability.

Fig. 3

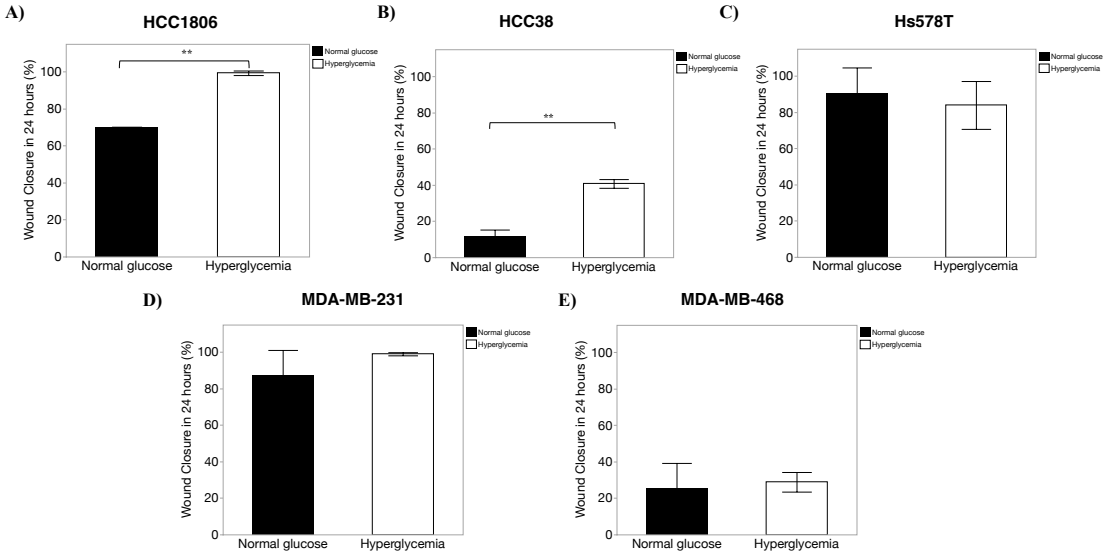

Figure 3 | Effect of Hyperglycemia on Wound Closure in TNBC Cell Lines. Percent wound closure at 24 h for (A) HCC1806 (normal glucose, $n = 2$; hyperglycemia, $n = 4$), (B) HCC38 ($n = 2$; $n = 3$), (C) Hs578T ($n = 3$; $n = 3$), (D) MDA-MB-231 ($n = 4$; $n = 3$), and (E) MDA-MB-468 ($n = 4$; $n = 3$). Bars show mean values; error bars denote ± s.d. from independent measurements. Statistical significance was assessed by two-tailed Student's *t*-test with unequal variance; $P < 0.05$.

In normal glucose conditions, significant differences in wound closure were observed among TNBC cell lines. HCC1806 exhibited greater wound closure compared to both HCC38 and MDA-MB-468. Conversely, HCC38 showed significantly reduced wound closure relative to Hs578T and MDA-MB-231. Hs578T also demonstrated greater wound closure than MDA-MB-468. Notably, the two pleural effusion–derived cell lines, MDA-MB-231 and MDA-MB-468, differed significantly, with MDA-MB-231 displaying higher wound closure than MDA-MB-468. (Fig. 4).

Fig. 4

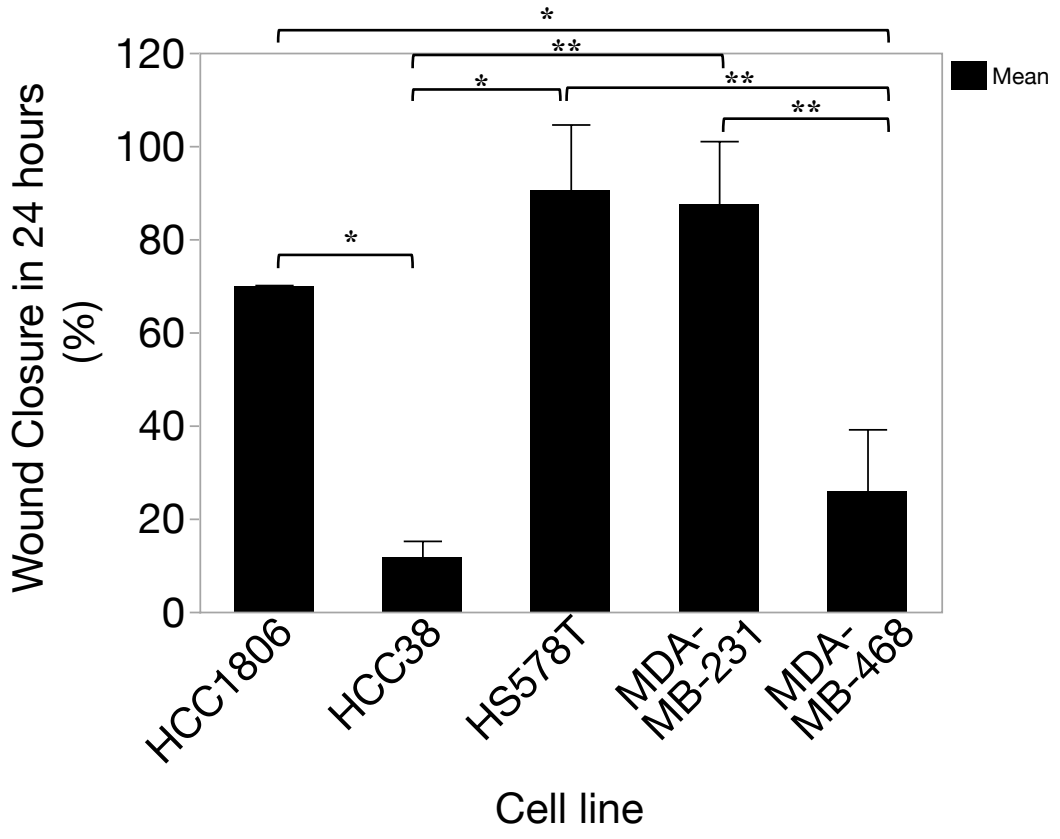

Figure 4 | Wound Closure of TNBC Cell Lines Under Normal Glucose Conditions at 24 h. Bars show mean values; error bars denote ± s.d. from independent measurements. Statistical significance was assessed using a two-tailed Student's *t*-test with unequal variance; $P < 0.05$

Under hyperglycemic conditions, similar patterns of wound closure were observed across TNBC cell lines. HCC1806 demonstrated significantly greater wound closure within 24 hours compared to HCC38 and MDA-MB-468. HCC38 displayed reduced wound closure relative to Hs578T and MDA-MB-231, though it remained higher than MDA-MB-468. Hs578T also exhibited significantly greater wound closure than MDA-MB-468. Among

the pleural effusion–derived lines, MDA-MB-231 closed wounds more effectively than MDA-MB-468 within 24 hours (Fig. 5).

Fig. 5

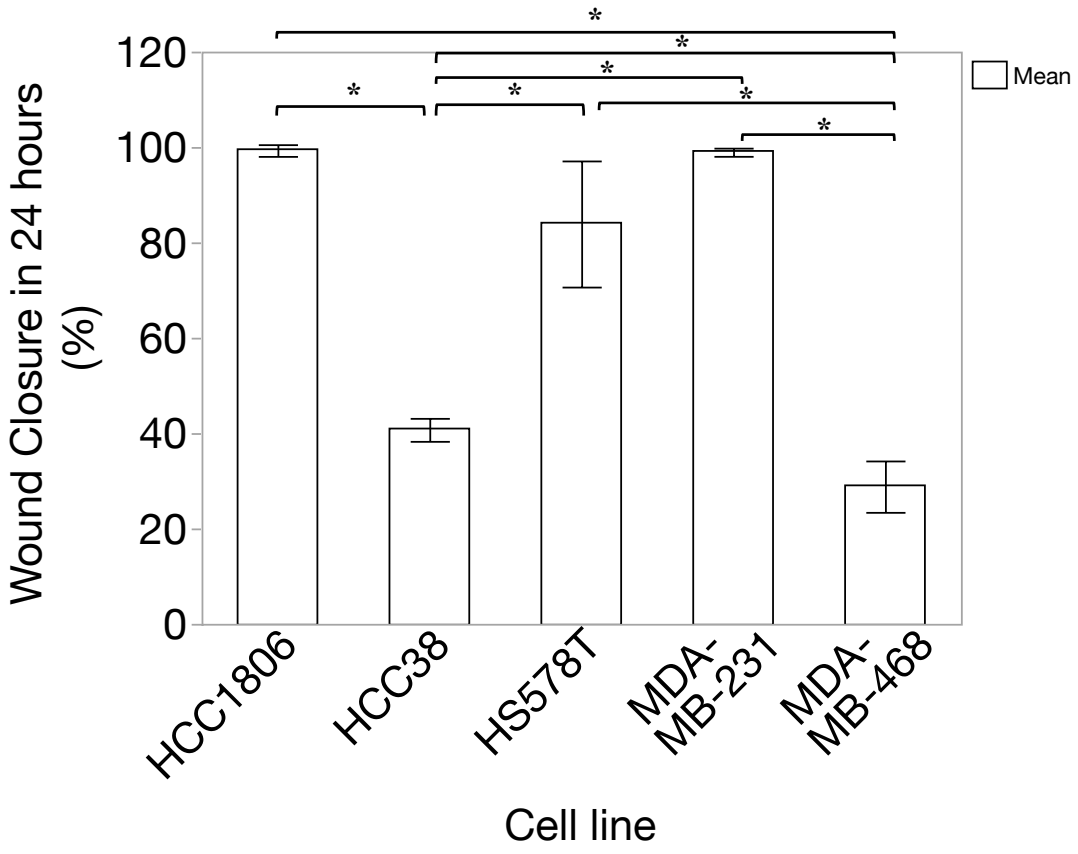

Figure 5 | Wound Closure of TNBC Cell Lines Under Hyperglycemia Conditions at 24 h. Bars show mean values; error bars denote ± s.d. from independent measurements. Statistical significance was assessed using a two-tailed Student's *t*-test with unequal variance; $P < 0.05$

These results suggest that, independent of glucose concentration, HCC1806, Hs578T, and MDA-MB-231 cells demonstrate a stronger capacity for wound closure migration, consistent with their more motile and invasive phenotypes. Their ability to efficiently

repopulate the denuded area of the monolayer after scratching implies that these cell lines have an intrinsically higher basal migratory potential that may contribute to their aggressive behavior in vivo. By contrast, HCC38 and MDA-MB-468 cells showed comparatively reduced wound closure, indicating that they possess a lower inherent migratory activity under the same culture conditions. The divergent responses between these groups of cell lines highlight heterogeneity within TNBC, suggesting that intrinsic differences in cytoskeletal dynamics, cell-cell adhesion, or signaling pathways regulating motility (e.g., PI3K/Akt, Ras/MAPK, or EMT-related transcription factors) may underlie the variation in scratch wound closure capacity. Importantly, the fact that these differences persisted regardless of glucose concentration indicates that while hyperglycemia may further modulate migratory potential, baseline motility traits remain a distinguishing feature of these TNBC subtypes. Fold differences between the cell lines are shown in table 2 in the appendix.

Limitations in this experiment included the relatively small number of biological replicates in certain conditions, such as HCC1806 and HCC38 under normoglycemic treatment, which reduces statistical power and limits confidence in the reproducibility of the observed trends. This makes it more difficult to determine whether differences in wound closure are truly representative of the biology of these cell lines or are influenced by experimental noise. Additionally, variability in the initial wound size across replicates could contribute to inconsistencies in the rate of wound closure, since a narrower or uneven scratch may artificially accelerate closure independent of true migratory capacity. The absence of parallel cell viability or proliferation assessments further complicates interpretation, as wound closure in this assay could reflect not only migration but also

differences in cell survival or division following the scratch. Without accounting for these confounding factors, it is challenging to fully disentangle whether the observed differences across cell lines and glucose conditions are due to intrinsic migratory potential, proliferative contributions, or artifacts introduced by assay variability.

3.1.3 Extracellular Matrix Attachment

Following the trans-well and scratch wound migration experiments, we next evaluated whether hyperglycemia alters TNBC cell attachment to extracellular matrix (ECM) proteins as a potential mechanism underlying the migratory phenotypes, particularly those observed in the scratch wound assay. Attachment assays were performed on collagen- and fibronectin-coated plates, and the percentage of cells that adhered after 30 minutes was quantified. Readings over 100% adhesion indicate potential cell loss at the 16-hour reading compared to the 30-minute plate reading. These ECM proteins were selected because they are major structural components of the tumor microenvironment and play a critical role in regulating cell adhesion, motility, and invasion. Stronger attachment to ECM proteins can facilitate more efficient migration by providing traction for cytoskeletal rearrangements, while weaker attachment may hinder directional movement. Based on this rationale, we hypothesized that hyperglycemia would increase ECM attachment in HCC1806 and HCC38 cells, consistent with their enhanced migration patterns in the scratch wound assay, and that little to no effect would be observed in Hs578T, MDA-MB-231, and MDA-MB-468.

On collagen, no significant differences in attachment were observed between glucose conditions for any of the cell lines, which was somewhat unexpected (Fig. 6). Interestingly, Hs578T, MDA-MB-231, and MDA-MB-468 displayed a trend toward

preferential attachment under normoglycemic conditions, although these differences did not reach statistical significance. This suggests that while collagen may support baseline adhesion in these cell lines, hyperglycemia does not appear to strongly modulate this interaction.

Fig. 6

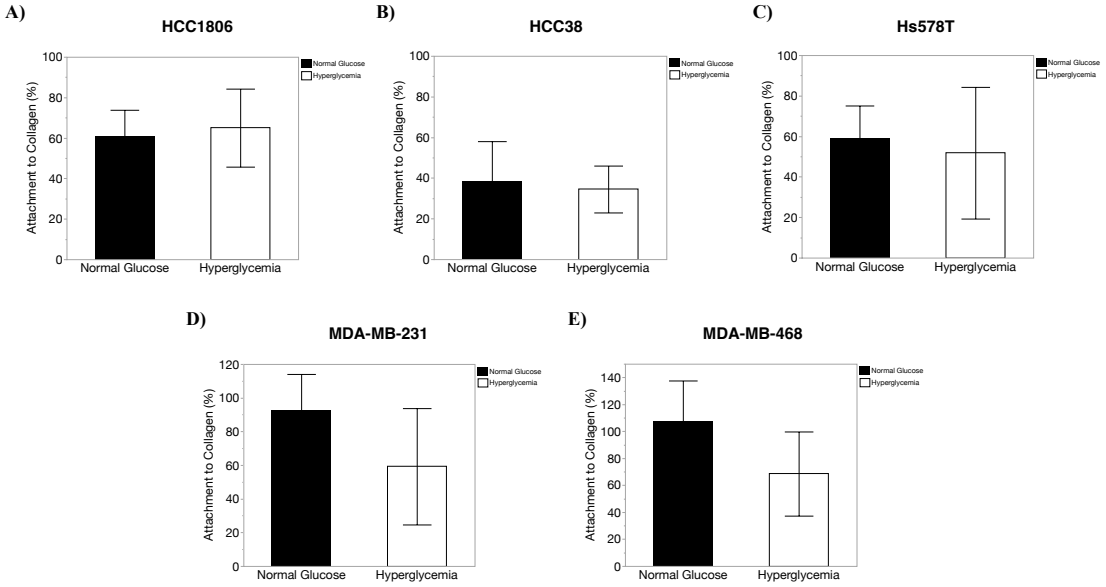

Figure 6 | Effect of Hyperglycemia on Collagen Attachment in TNBC Cell Lines. Percent collagen adhesion after 30 min in (A) HCC1806 ($n = 5$, normal glucose; $n = 6$, hyperglycemia), (B) HCC38 ($n = 4$; $n = 8$), (C) Hs578T ($n = 3$; $n = 4$), (D) MDA-MB-231 ($n = 3$; $n = 6$), and (E) MDA-MB-468 ($n = 3$; $n = 4$). Bars show mean values; error bars denote ± s.d. from independent measurements. Statistical significance was assessed using a two-tailed Student's *t*-test with unequal variance; $P < 0.05$.

However, intercellular comparisons revealed significantly higher adhesion in HCC1806 relative to HCC38 under hyperglycemia, and HCC38 exhibited reduced adhesion compared to MDA-MB-231 and MDA-MB-468 (Fig. 7).

Fig. 7

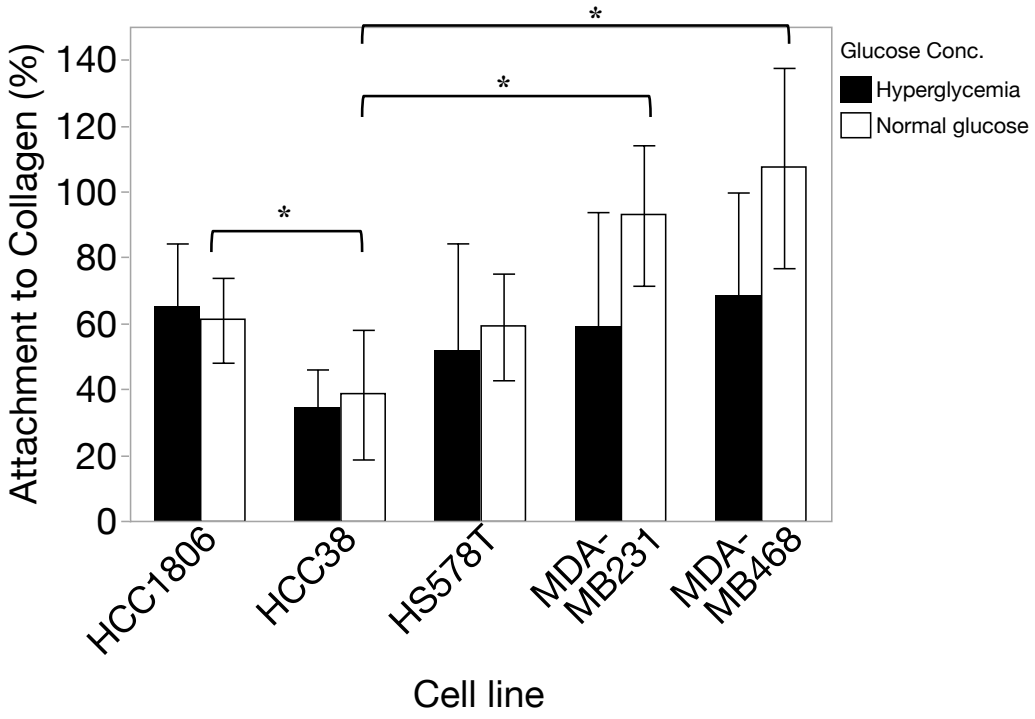

Figure 7 | Collagen Adhesion of TNBC Cell Lines Under Normal Glucose and Hyperglycemic Conditions. Bars show mean values; error bars denote ± s.d. from independent measurements. Statistical significance was assessed using a two-tailed Student's *t*-test with unequal variance; $P < 0.05$.

On fibronectin, as with collagen, glucose conditions did not significantly alter adhesion within any of the cell lines (Fig. 8). However, non-significant trends were observed in which HCC1806 and Hs578T showed greater attachment under hyperglycemic conditions, whereas HCC38, MDA-MB-231, and MDA-MB-468 exhibited a tendency toward increased attachment in normoglycemia.

Fig. 8

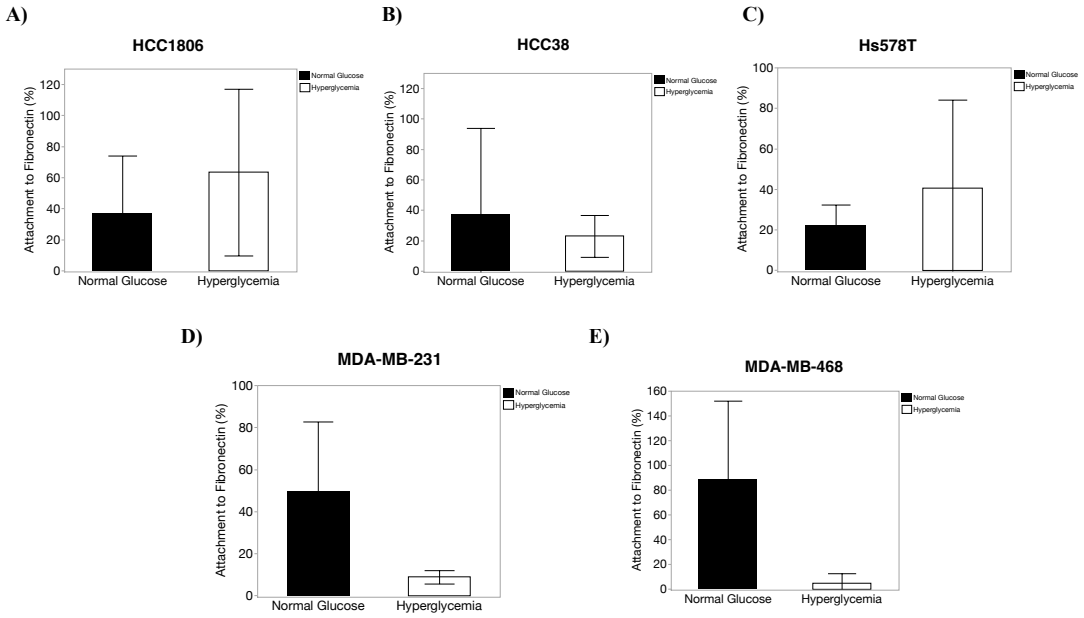

Figure 8 | Effect of Hyperglycemia on Fibronectin Attachment in TNBC Cell Lines. Percent collagen adhesion after 30 min in (A) HCC1806 ($n = 6$, normal glucose; $n = 6$, hyperglycemia), (B) HCC38 ($n = 3$; $n = 7$), (C) Hs578T ($n = 3$; $n = 4$), (D) MDA-MB-231 ($n = 4$; $n = 4$), and (E) MDA-MB-468 ($n = 4$; $n = 3$). Bars show mean values; error bars denote ± s.d. from independent measurements. Statistical significance was assessed using a two-tailed Student's *t*-test with unequal variance; $P < 0.05$.

However, comparing between the TNBC cell lines, HCC1806 displayed significantly greater adhesion relative to MDA-MB-468, and HCC38 adhered more strongly than MDA-MB-231 and MDA-MB-468 under hyperglycemia (Fig. 9).

Fig. 9

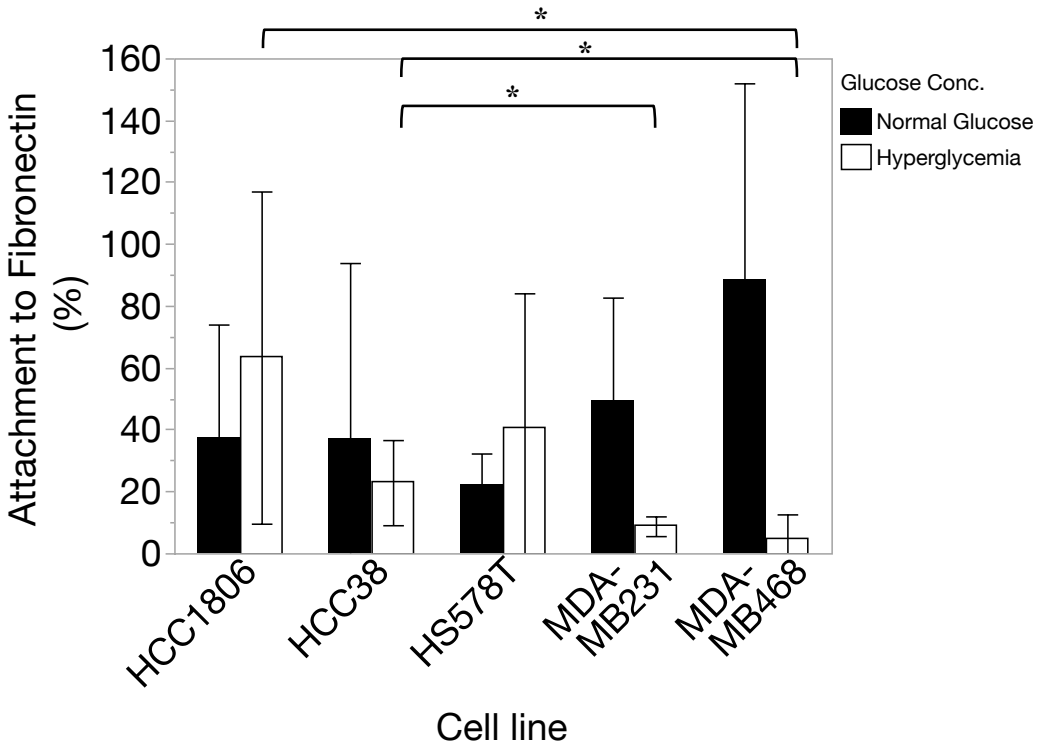

Figure 9 | Fibronectin Adhesion of TNBC Cell Lines Under Normal Glucose and Hyperglycemic Conditions. Bars show mean values; error bars denote ± s.d. from independent measurements. Statistical significance was assessed using a two-tailed Student's t-test with unequal variance; $P < 0.05$.

Overall, hyperglycemia did not uniformly alter adhesion to either ECM protein across the TNBC cell lines tested. Instead, the data revealed that differences were more pronounced between cell lines themselves, underscoring the intrinsic heterogeneity that characterizes

TNBC. This variability likely reflects differences in integrin expression profiles, cytoskeletal organization, or intracellular signaling pathways that govern adhesion dynamics. Such cell line–specific patterns highlight that while glucose availability may modulate adhesion in certain contexts, the baseline adhesive properties of each subtype remain a dominant determinant. These findings are consistent with the broader theme of TNBC heterogeneity, where functional responses to microenvironmental cues can diverge substantially across models. Fold differences between the cell lines for collagen and fibronectin are shown in table 3 and 4 respectively in the appendix.

The interpretation of these results is also limited by several experimental factors. The absence of viability assays makes it difficult to rule out the possibility that reduced adhesion in some conditions was due to impaired cell survival rather than altered integrin–ECM binding. Additionally, variability across replicates reduced the statistical strength of the findings, making subtle effects of glucose on adhesion difficult to resolve. Future experiments incorporating viability controls, larger sample sizes, and integrin-blocking strategies could help disentangle whether the observed adhesion patterns are driven by true changes in adhesive signaling or confounded by cell survival and experimental variability.

3.1.4 Cell Accumulation – Glucose-Dependent Growth Dynamics

To assess the impact of glucose on cell growth as another indicator of breast cancer aggressiveness, we monitored cell accumulation over several days. Faster accumulation rates are typically associated with a more aggressive phenotype, reflecting enhanced survival, proliferative capacity, and metabolic adaptability, while slower accumulation suggests a less aggressive profile. This relationship is closely tied to the Warburg effect,

in which cancer cells preferentially utilize glycolysis for energy production even in the presence of oxygen. By relying heavily on glucose metabolism, highly aggressive tumors can rapidly generate both ATP and biosynthetic intermediates needed to sustain proliferation. In this context, hyperglycemia provides a readily available fuel source that may amplify the glycolytic advantage of TNBC cells, driving enhanced accumulation as a functional readout of aggressiveness. Based on this rationale, we hypothesized that exposure to hyperglycemia would promote proliferation-like accumulation across all TNBC cell lines, though the magnitude of this effect could vary according to each line's inherent metabolic programming.

HCC1806 displayed accelerated accumulation under hyperglycemia, reaching significance at day 3 (Fig. 10A). Hs578T trended toward faster growth in hyperglycemia without reaching significance (Fig. 10B). MDA-MB-231 showed a significant increase at day 4 (Fig. 10C), whereas MDA-MB-468 showed no glucose-dependent differences (Fig. 10D). The overall trend across all TNBC cell lines lends to higher cell accumulation in hyperglycemia compared to normal glucose.

Fig. 10

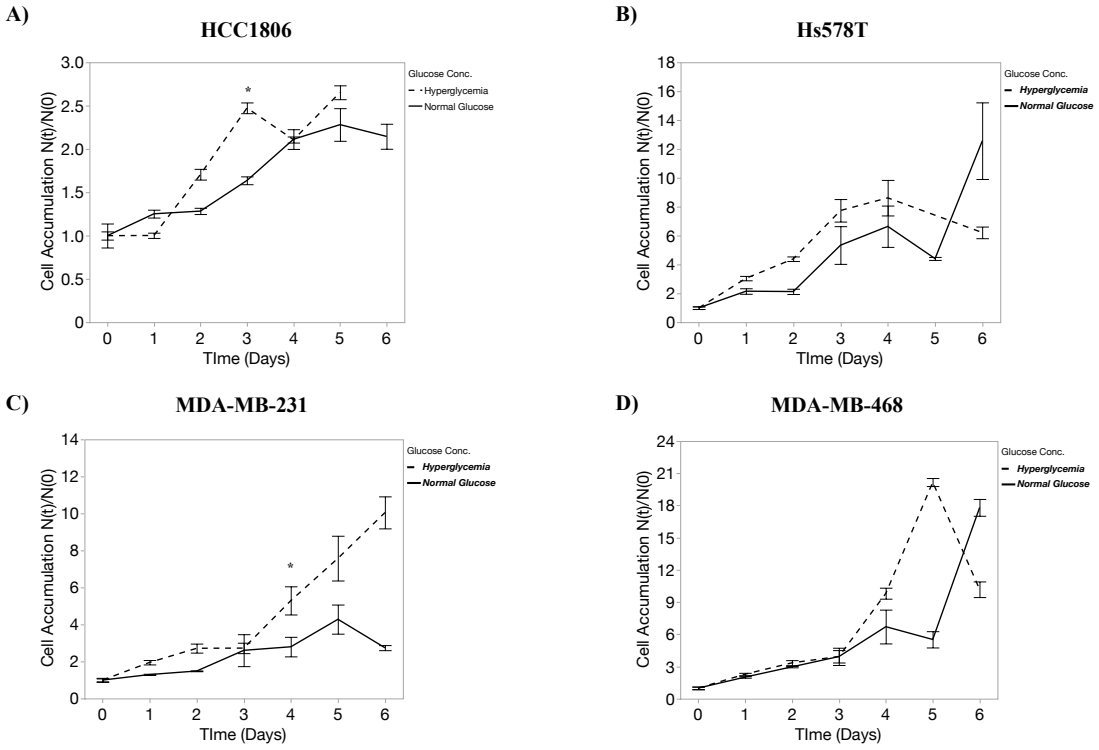

Figure 10 | Effect of Hyperglycemia on Cell Accumulation in TNBC Cell Lines. Cell accumulation over time, normalized to day 0, in (A) HCC1806 ($n = 5$, normal glucose; $n = 5$, hyperglycemia for each day), (B) HCC38 ($n = 5$; $n = 5$), (C) Hs578T ($n = 5$; $n = 5$), (D) MDA-MB-231 ($n = 5$; $n = 5$), and (E) MDA-MB-468 ($n = 5$; $n = 5$). Line graphs represent mean values; error bars indicate ± s.d. from independent measurements. Statistical significance was determined using a two-tailed Student's *t*-test with unequal variance for each day; $P < 0.05$.

Further analysis compared cell accumulation across TNBC cell lines under both glucose conditions. In normoglycemia, HCC38 and MDA-MB-468 showed a significant increase in cell accumulation compared to HCC1806 on days one, two, and five (Fig. 11). Additionally, on day two, MDA-MB-468 exhibited significantly greater accumulation than both Hs578T and MDA-MB-231.

Fig. 11

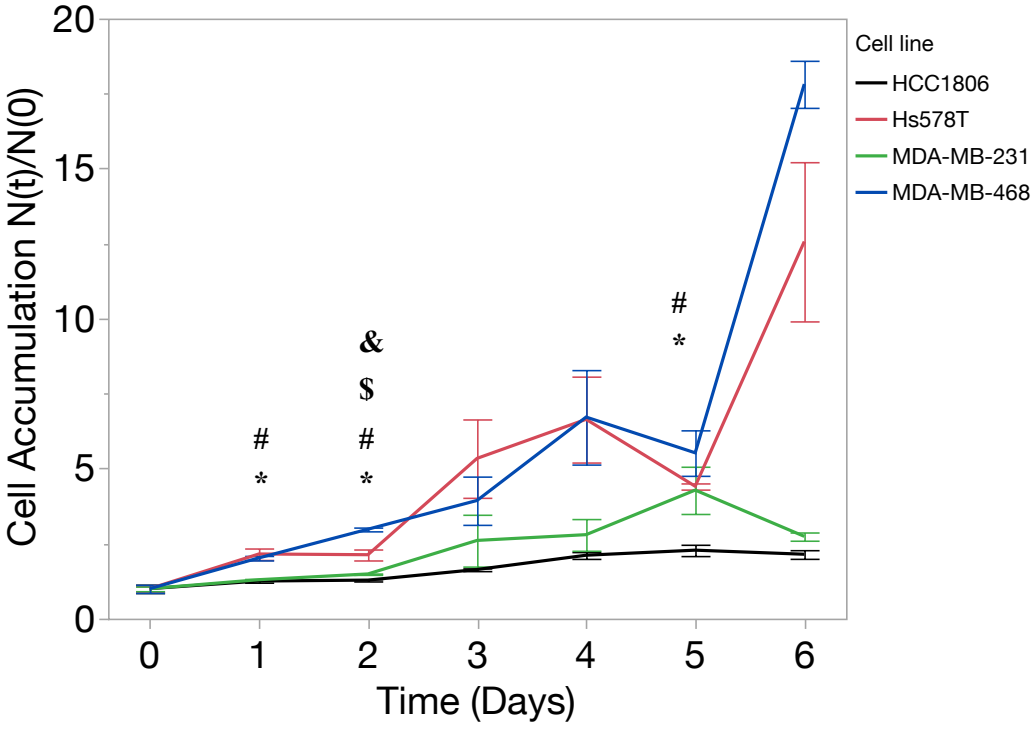

Figure 11 | Cell Accumulation of TNBC Cell Lines Under Normal Glucose Conditions. Line graphs represent mean values; error bars indicate ± s.d. from independent measurements. Statistical significance was determined using a two-tailed Student's *t*-test with unequal variance for each day ($P < 0.05$). * Denotes a significant difference between HCC1806 and Hs578T; # denotes a significant difference between HCC1806 and MDA-MB-468; $ denotes a significant difference between Hs578T and MDA-MB-468; and & denotes a significant difference between MDA-MB-231 and MDA-MB-468.

In hyperglycemia, Hs578T and MDA-MB-468 showed a significant increase in cell accumulation on day one compared to HCC1806. By day five, MDA-MB-231 also demonstrated significantly greater accumulation relative to HCC1806 (Fig. 12).

Fig. 12

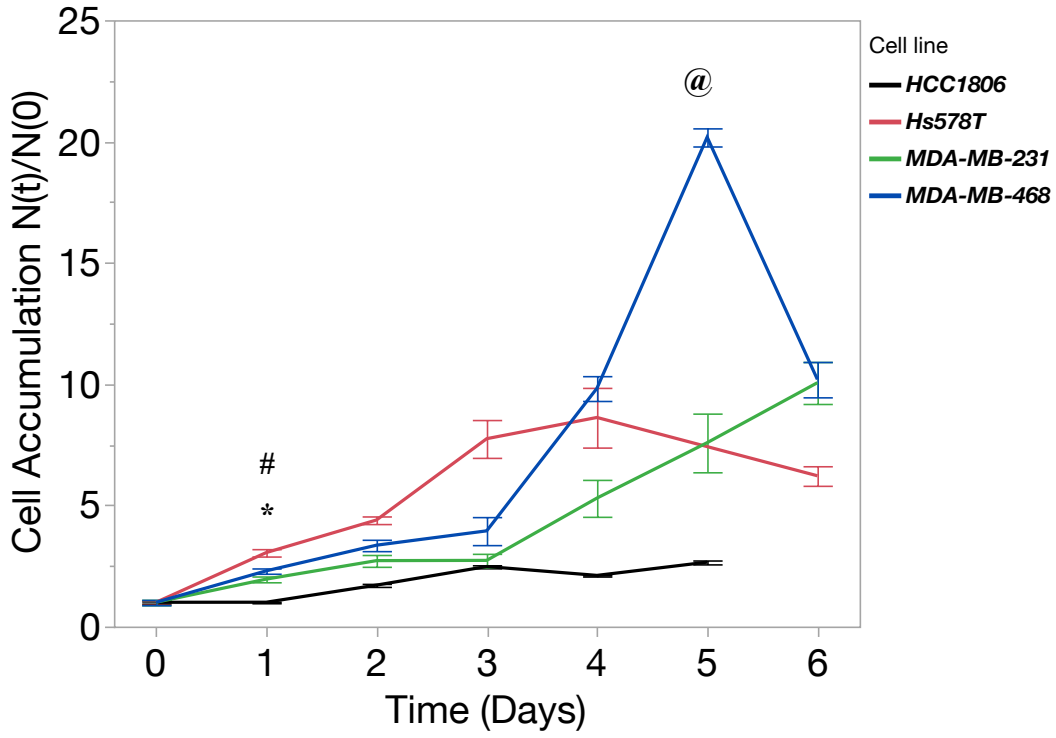

Figure 12 | Cell Accumulation of TNBC Cell Lines Under Hyperglycemia Conditions. Line graphs represent mean values; error bars indicate ± s.d. from independent measurements. Statistical significance was determined using a two-tailed Student's *t*-test with unequal variance for each day ($P < 0.05$). * Denotes a significant difference between HCC1806 and Hs578T; @ denotes a significant difference between MDA-MB-231 and MDA-MB-468.

Hyperglycemia appeared to promote faster cell accumulation in certain TNBC subtypes, though this effect was not uniform across all lines. HCC1806 and MDA-MB-231 were particularly responsive, suggesting that these cells may derive a metabolic advantage from elevated glucose availability, potentially through enhanced glycolytic activity consistent with Warburg-like metabolism. In contrast, MDA-MB-468 showed little

sensitivity to glucose levels, underscoring subtype-specific differences in how TNBC cells exploit metabolic resources. Fold differences between the cell lines are shown in table 5 in the appendix.

It is important to note that cell accumulation reflects net changes in cell number rather than direct proliferation alone, meaning that differential survival or cell death could also contribute to the observed patterns. These findings highlight the complexity of glucose-driven phenotypes in TNBC and emphasize the need for complementary assays to disentangle proliferation from survival effects.

3.2 Altered Phosphatidylinositol Composition in TNBC Under Hyperglycemia

To determine whether glucose-driven phenotypic changes are accompanied by alterations in lipid signaling, we quantified phosphatidylinositol phosphates (PIPs) in plasma membrane–derived vesicles (GPMVs). The GPMV assay provides a powerful tool for isolating and studying the lipid composition of the plasma membrane independent of cytoskeletal and intracellular influences, offering a direct window into membrane organization and signaling potential. Because GPMVs preserve the native lipid environment, they are especially well-suited for quantifying bioactive lipids such as PIPs, which serve as key regulators of cytoskeletal remodeling, vesicle trafficking, and cell migration. Beyond targeted lipid analysis, GPMVs can also be integrated into lipidomic workflows, allowing for comprehensive profiling of membrane lipid species and their dynamic remodeling under different conditions. In the context of hyperglycemia and TNBC, this approach enables the interrogation of how metabolic stress influences membrane lipid signaling networks, potentially linking altered lipid homeostasis to the aggressive phenotypes observed in migration and accumulation assays.

In HCC38 cells, hyperglycemia did not significantly alter the plasma membrane distribution of phosphatidylinositol phosphates, with average levels of PI, PI(4)P, PI(5)P, $PI(3,4)P_2$, $PI(4,5)P_2$, and $PI(3,4,5)P_3$ remaining within the 15–20% range across all derivatives (Figure 13A–F).

Fig. 13

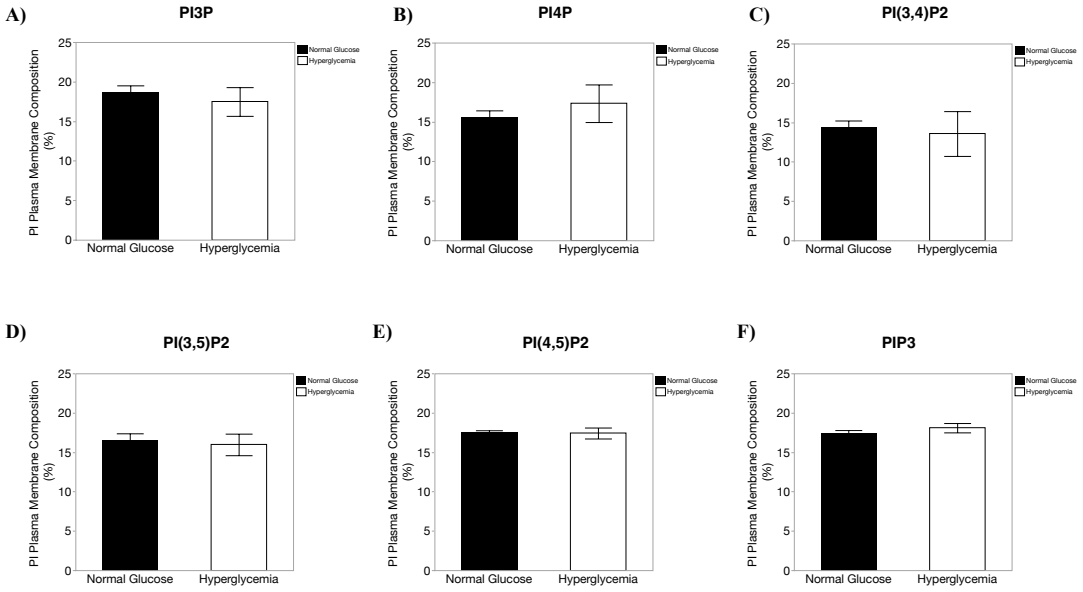

Figure 13 | Effect of Hyperglycemia on Phosphatidylinositol Phosphate (PIP) Composition in Giant Plasma Membrane Vesicles (GPMVs) from HCC38 Cells. Percent plasma membrane composition of (A) PI3P ($n = 3$, normal glucose; $n = 8$, hyperglycemia), (B) PI4P ($n = 3$; $n = 8$), (C) $PI(3,4)P_2$ ($n = 3$; $n = 8$), (D) $PI(3,5)P_2$ ($n = 3$; $n = 8$), (E) $PI(4,5)P_2$ ($n = 3$; $n = 8$), and (F) PIP_3 ($n = 3$; $n = 8$) under normal glucose and hyperglycemic conditions. Bars represent mean values; error bars denote ± s.d. from independent measurements. Statistical significance was assessed using a two-tailed Student's *t*-test with unequal variance ($P < 0.05$).

In Hs578T cells, hyperglycemia did not significantly alter the plasma membrane distribution of phosphatidylinositol phosphates, with average levels of PI, PI(4)P, PI(5)P, $PI(4,5)P_2$, and $PI(3,4,5)P_3$ remaining around 20% across both glucose conditions, while $PI(3,4)P_2$ was consistently lower at approximately 7% (Figure 14A–F).

Fig. 14

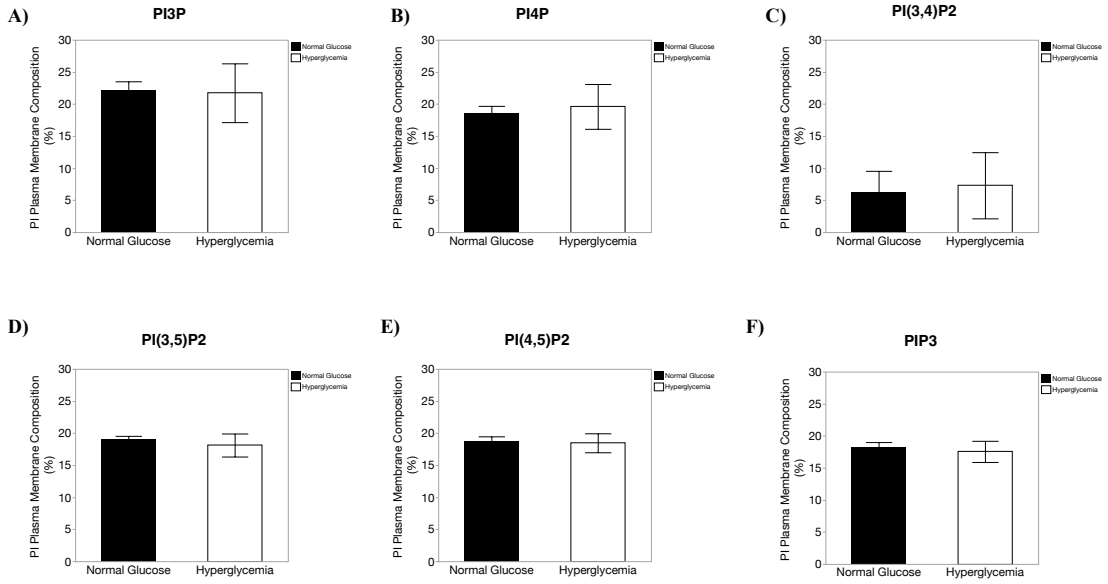

Figure 14 | Effect of Hyperglycemia on Phosphatidylinositol Phosphate (PIP) Composition in Giant Plasma Membrane Vesicles (GPMVs) from Hs578T Cells. Percent plasma membrane composition of (A) PI3P ($n = 5$, normal glucose; $n = 6$, hyperglycemia), (B) PI4P ($n = 5$; $n = 6$), (C) $PI(3,4)P_2$ ($n = 5$; $n = 6$), (D) $PI(3,5)P_2$ ($n = 5$; $n = 6$), (E) $PI(4,5)P_2$ ($n = 5$; $n = 6$), and (F) PIP_3 ($n = 5$; $n = 6$) under normal glucose and hyperglycemic conditions. Bars represent mean values; error bars denote ± s.d. from independent measurements. Statistical significance was assessed using a two-tailed Student's *t*-test with unequal variance ($P < 0.05$).

In MDA-MB-231 cells, hyperglycemia did not significantly alter the plasma membrane distribution of phosphatidylinositol phosphates, with average levels of PI, PI(4)P, PI(5)P, $PI(4,5)P_2$, and $PI(3,4,5)P_3$ remaining around 20% under both glucose conditions, while $PI(3,4)P_2$ was consistently lower at approximately 8% (Figure 15A–F).

Fig. 15

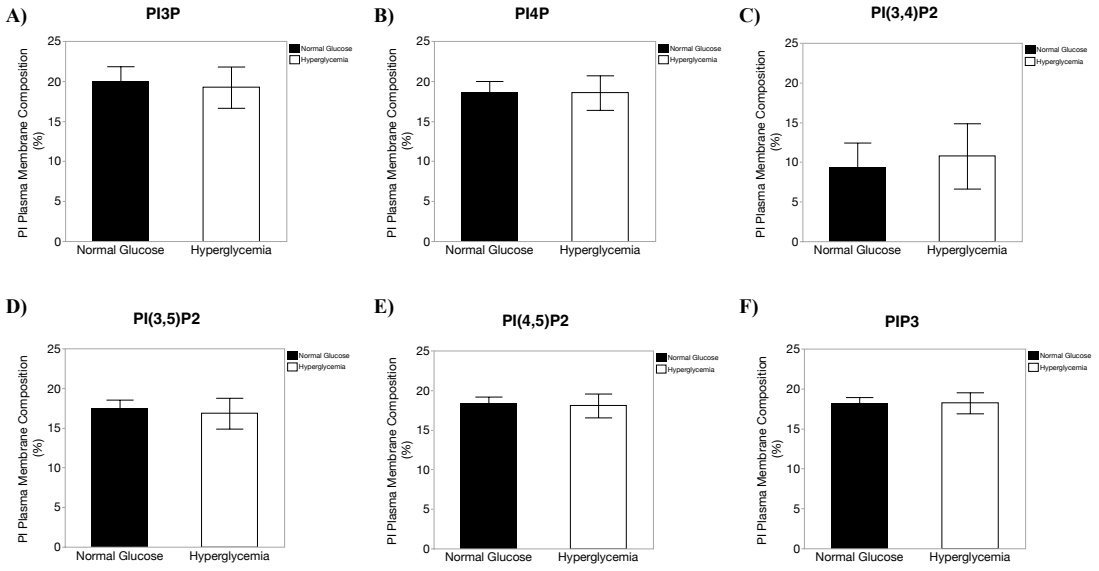

Figure 15 | Effect of Hyperglycemia on Phosphatidylinositol Phosphate (PIP) Composition in Giant Plasma Membrane Vesicles (GPMVs) from MDA-MB-231 Cells. Percent plasma membrane composition of (A) PI3P ($n = 14$, normal glucose; $n = 9$, hyperglycemia), (B) PI4P ($n = 14$; $n = 9$), (C) $PI(3,4)P_2$ ($n = 14$; $n = 9$), (D) $PI(3,5)P_2$ ($n = 14$; $n = 9$), (E) $PI(4,5)P_2$ ($n = 14$; $n = 9$), and (F) PIP_3 ($n = 14$; $n = 9$) under normal glucose and hyperglycemic conditions. Bars represent mean values; error bars denote ± s.d. from independent measurements. Statistical significance was assessed using a two-tailed Student's *t*-test with unequal variance ($P < 0.05$).

In MDA-MB-468 cells, hyperglycemia did not significantly alter the plasma membrane distribution of phosphatidylinositol phosphates, with average levels of PI, PI(4)P, PI(5)P, $PI(4,5)P_2$, and $PI(3,4,5)P_3$ remaining around 20% under both glucose conditions, while $PI(3,4)P_2$ was consistently lower at approximately 8% (Figure 16A–F).

Fig. 16

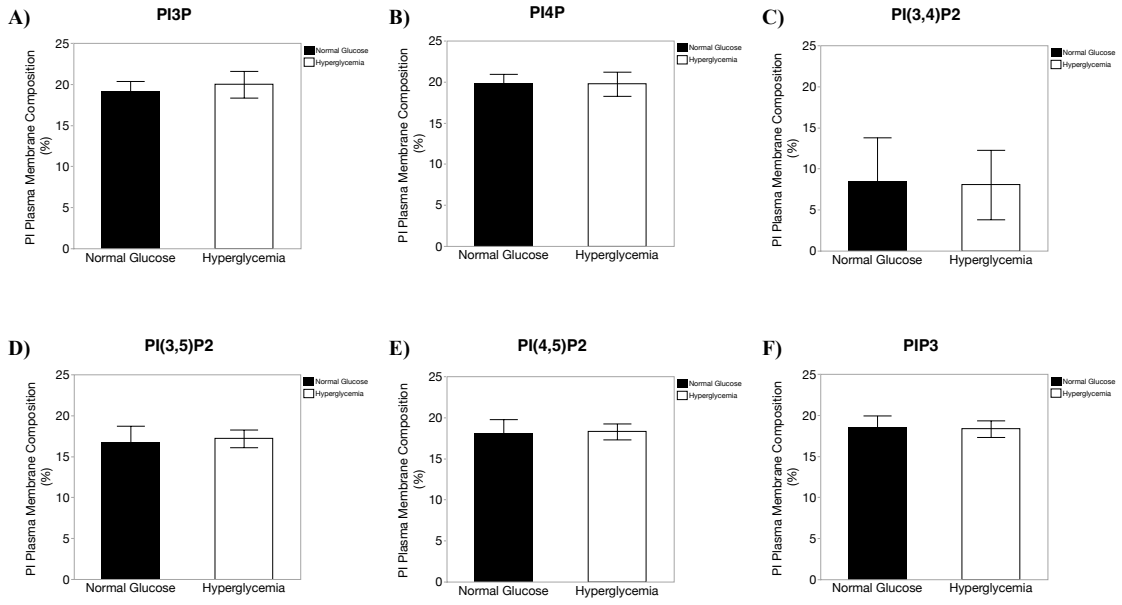

Figure 16 | Effect of Hyperglycemia on Phosphatidylinositol Phosphate (PIP) Composition in Giant Plasma Membrane Vesicles (GPMVs) from MDA-MB-468 Cells. Percent plasma membrane composition of (A) PI3P ($n = 4$, normal glucose; $n = 8$, hyperglycemia), (B) PI4P ($n = 4$; $n = 8$), (C) $PI(3,4)P_2$ ($n = 4$; $n = 8$), (D) $PI(3,5)P_2$ ($n = 4$; $n = 8$), (E) $PI(4,5)P_2$ ($n = 4$; $n = 8$), and (F) PIP_3 ($n = 4$; $n = 8$) under normal glucose and hyperglycemic conditions. Bars represent mean values; error bars denote ± s.d. from independent measurements. Statistical significance was assessed using a two-tailed Student's *t*-test with unequal variance ($P < 0.05$).

Further analysis of PIP accumulation across TNBC cell lines revealed several significant differences under both glucose conditions. In normal glucose, HCC38 exhibited significantly lower PI3P accumulation compared to Hs578T, which itself showed higher levels than MDA-MB-231 and MDA-MB-468. Under hyperglycemia, HCC38 only showed reduced PI3P relative to MDA-MB-468 (Fig. 17A). A similar pattern was observed for PI4P, where HCC38 had lower accumulation compared to Hs578T, MDA-MB-231, and MDA-MB-468 in normoglycemia, but only compared to MDA-MB-468 in hyperglycemia (Fig. 17B). By contrast, HCC38 showed significantly higher $PI(3,4)P_2$ accumulation than Hs578T and MDA-MB-231 in normal glucose, and higher levels than Hs578T and MDA-MB-468 in hyperglycemia (Fig. 17C). For $PI(3,5)P_2$, HCC38 displayed lower accumulation than Hs578T under both glucose conditions, while Hs578T had higher levels than MDA-MB-231 only in normoglycemia (Fig. 17D). HCC38 also exhibited reduced $PI(4,5)P_2$ accumulation compared to Hs578T and MDA-MB-231 in normal glucose, although no differences were observed among the lines under hyperglycemia (Fig. 17E). Finally, HCC38 showed lower PIP_3 accumulation compared to MDA-MB-231 in normoglycemia, but no significant differences in PIP_3 levels were detected among the cell lines under hyperglycemia (Fig. 17F).

Fig. 17

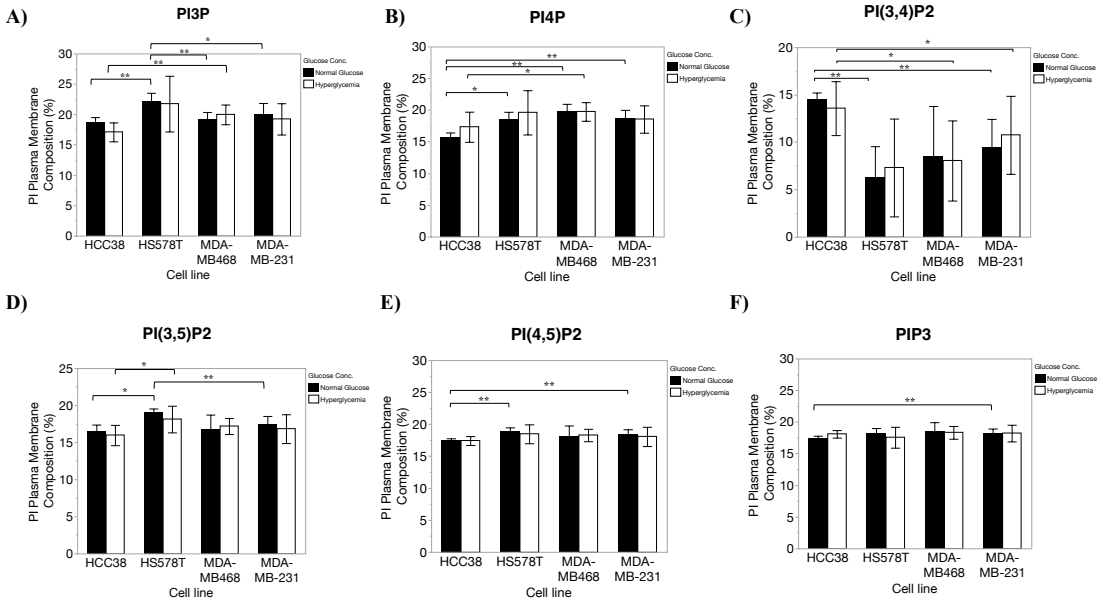

Figure 17 | Phosphatidylinositol Phosphate (PIP) Composition in Giant Plasma Membrane Vesicles (GPMVs) of TNBC Cell Lines in Normal Glucose and Hyperglycemia. Percent plasma membrane composition of (A) PI3P (B) PI4P (C) $PI(3,4)P_2$ (D) $PI(3,5)P_2$ (E) $PI(4,5)P_2$ and (F) PIP_3 under normal glucose and hyperglycemic conditions. Bars represent mean values; error bars denote ± s.d. from independent measurements. Statistical significance was assessed using a two-tailed Student's *t*-test with unequal variance ($P < 0.05$).

Hyperglycemia does not appear to directly remodel PIP composition within TNBC cell lines, but clear inter-cell line differences suggest that each subtype maintains distinct PIP profiles that may shape its signaling landscape. Since PIPs act as key regulators of pathways controlling cytoskeletal remodeling, membrane trafficking, and survival, even subtle differences in their steady-state distribution could have profound effects on how cells respond to external cues. For example, elevated $PI(3,4)P_2$ in HCC38 may bias these

cells toward altered PI3K/Akt or Rac1-driven motility, whereas higher PI4P or PI(4,5)P_2 in other lines could favor integrin-mediated adhesion and migration. These findings highlight that lipid signaling heterogeneity, rather than glucose itself, may be a major determinant of the divergent phenotypes observed across TNBC subtypes. Fold differences between the cell lines across all PIP derivatives are shown in tables 6 -11 in the appendix.

3.3 PIP Antibody Screening – Toward a Biomarker Strategy

To evaluate the potential of PIPs as biomarkers, we performed a high-throughput antibody-based screen across non-breast cancer cells and TNBC cell lines under both glucose conditions. While PIPs are predominantly localized to the inner leaflet of the plasma membrane where they regulate intracellular signaling, several studies have demonstrated that specific PIP derivatives can also be detected on the outer leaflet. This external localization is thought to arise from their bulky headgroups, which influence membrane curvature and allow limited asymmetric distribution even in the absence of active flipases or flopases [56]. For example, PI(4,5)P_2 has been detected on the outer leaflet of non-permeabilized cells, where it contributes to adhesion and cytoskeletal dynamics [57], and PI3P has been reported on the platelet cell surface [58]. Building on this evidence, we reasoned that a live-cell antibody screen could provide insight into whether PIPs differentially accumulate on the surface of aggressive TNBC subtypes, thereby identifying novel opportunities for detection, therapeutic targeting, or stratification of disease.

In this experiment, we included non-breast cancer cell lines, HEK293T and KTB36, to serve as comparators for evaluating the PIP biomarker potential of aggressive TNBC

subtypes. In HEK293T cells, no significant differences in antibody binding were observed between normoglycemic and hyperglycemic conditions (Figs. 18A–F).

Fig. 18

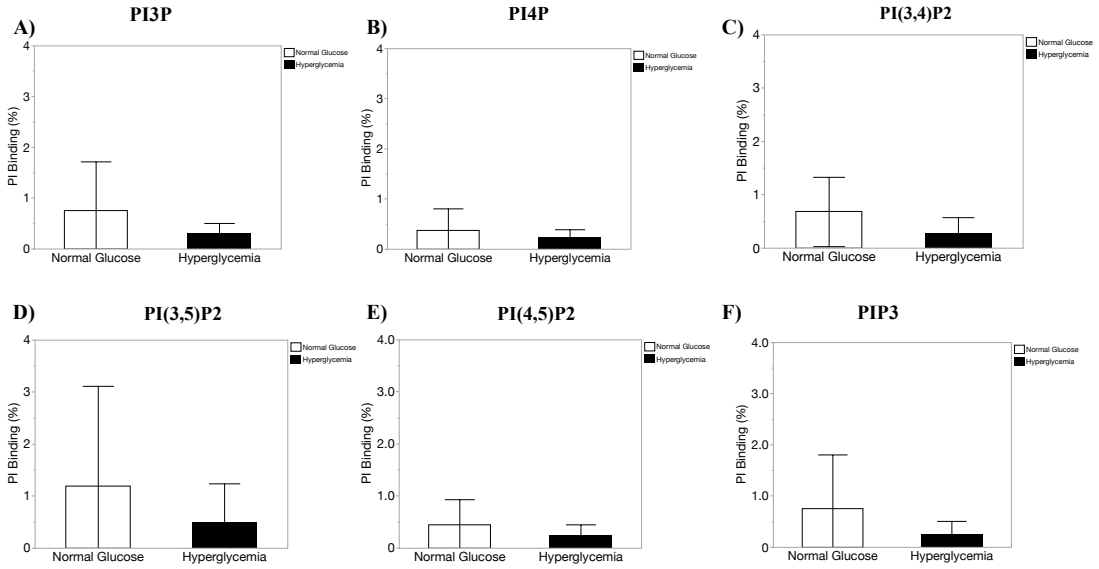

Figure 18 | HEK293T PIP Antibody Binding in Normal Glucose and Hyperglycemia. Antibody binding intensity, expressed as a percentage of the total number of NIR680-labeled cells, for (A) PI3P ($n = 4$, normal glucose; $n = 4$, hyperglycemia), (B) PI4P ($n = 4$; $n = 4$), (C) PI(3,4)P_2 ($n = 4$; $n = 4$), (D) PI(3,5)P_2 ($n = 4$; $n = 4$), (E) PI(4,5)P_2 ($n = 4$; $n = 4$), and (F) PIP_3 ($n = 4$; $n = 4$) under normal glucose and hyperglycemic conditions. Bars represent mean values; error bars denote ± s.d. from independent measurements. Statistical significance was determined using a two-tailed Student's *t*-test with unequal variance ($P < 0.05$).

Within non-breast cancer KTB36 cell lines, no significant differences in antibody binding were observed between normal glucose and hyperglycemia either (Figs. 19A-F).

Fig. 19

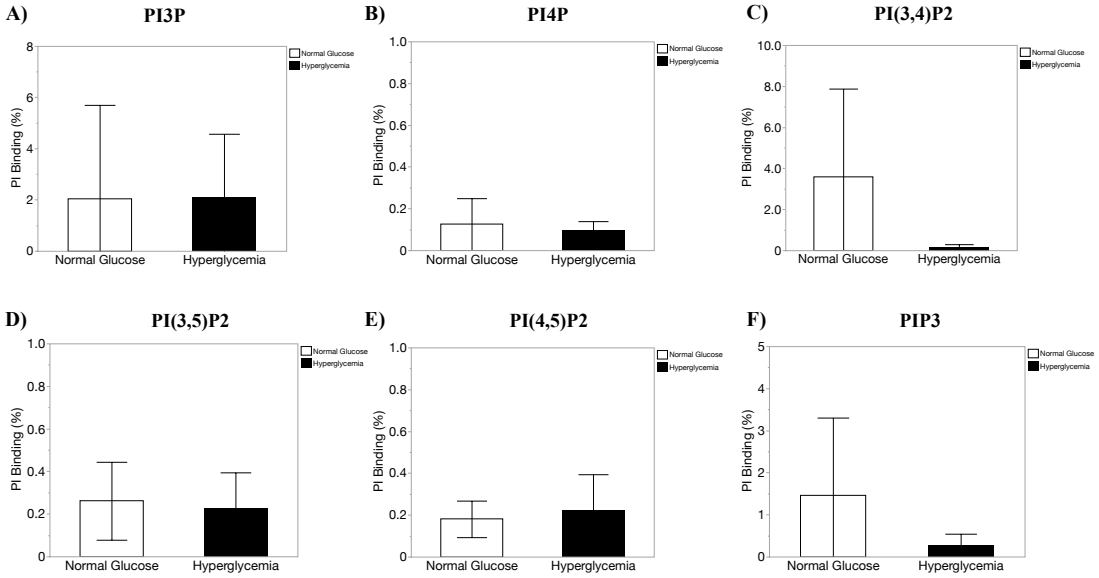

Figure 19 | KTB36 PIP Antibody Binding in Normal Glucose and Hyperglycemia. Antibody binding intensity, expressed as a percentage of the total number of NIR680-labeled cells, for (A) PI3P ($n = 4$, normal glucose; $n = 4$, hyperglycemia), (B) PI4P ($n = 4$; $n = 4$), (C) PI(3,4)P_2 ($n = 4$; $n = 4$), (D) PI(3,5)P_2 ($n = 4$; $n = 4$), (E) PI(4,5)P_2 ($n = 4$; $n = 4$), and (F) PIP_3 ($n = 4$; $n = 4$) under normal glucose and hyperglycemic conditions. Bars represent mean values; error bars denote ± s.d. from independent measurements. Statistical significance was determined using a two-tailed Student's *t*-test with unequal variance ($P < 0.05$).

In the TNBC cell line HCC1806, and consistent with GPMV observations, no significant differences in antibody binding were detected between normoglycemic and hyperglycemic conditions (Figs. 20A–F).

Fig. 20

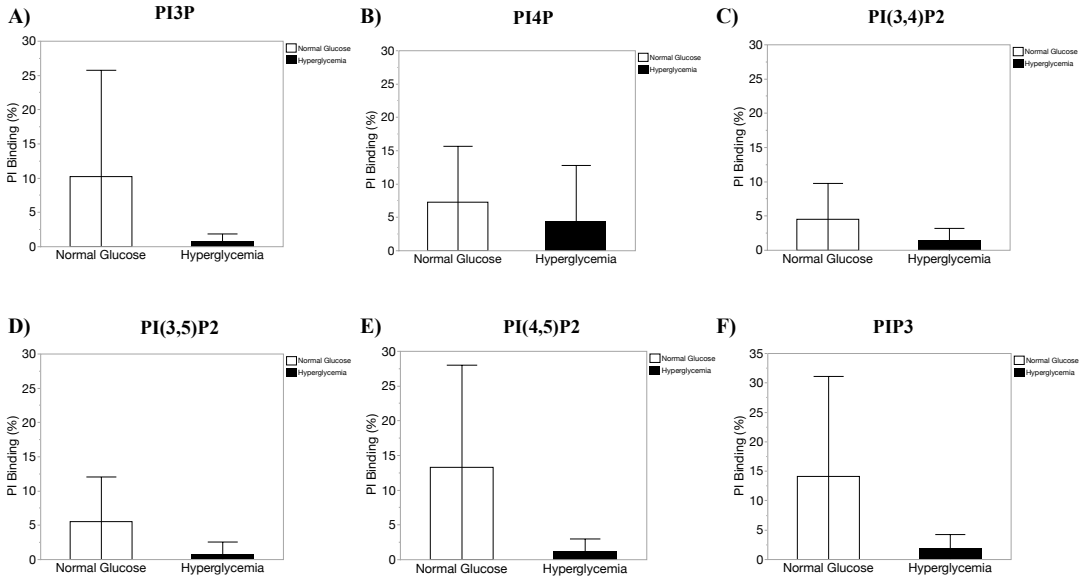

Figure 20 | HCC1806 PIP Antibody Binding in Normal Glucose and Hyperglycemia. Antibody binding intensity, expressed as a percentage of the total number of NIR680-labeled cells, for (A) PI3P ($n = 5$, normal glucose; $n = 5$, hyperglycemia), (B) PI4P ($n = 5$; $n = 5$), (C) PI(3,4)P_2 ($n = 5$; $n = 5$), (D) PI(3,5)P_2 ($n = 5$; $n = 5$), (E) PI(4,5)P_2 ($n = 5$; $n = 5$), and (F) PIP_3 ($n = 5$; $n = 5$) under normal glucose and hyperglycemic conditions. Bars represent mean values; error bars denote ± s.d. from independent measurements. Statistical significance was determined using a two-tailed Student's *t*-test with unequal variance ($P < 0.05$).

Within TNBC HCC38 cell lines, no significant differences in antibody binding were observed between normal glucose and hyperglycemia (Figs. 21A-F).

Fig. 21

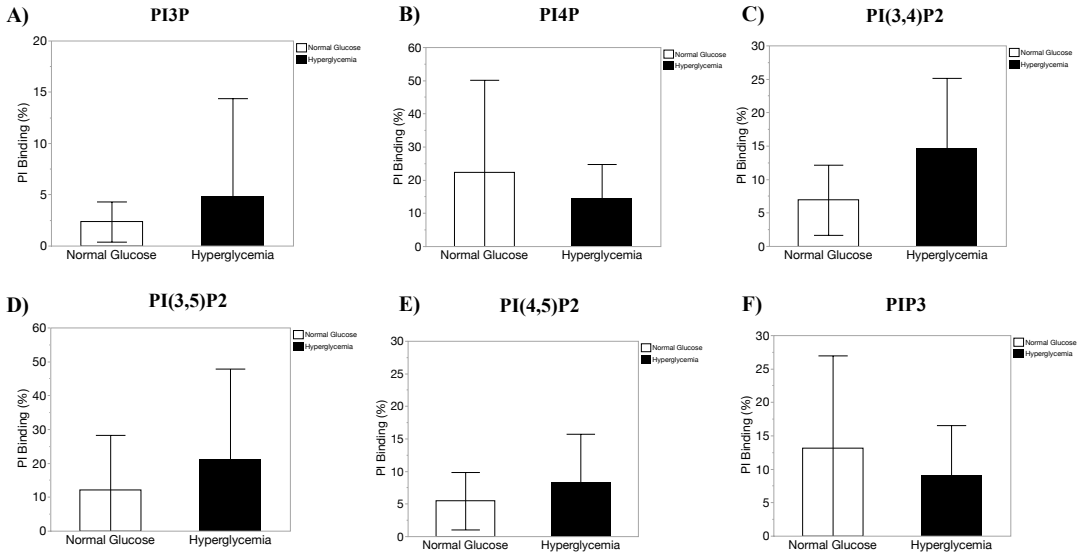

Figure 21 | HCC38 PIP Antibody Binding in Normal Glucose and Hyperglycemia. Antibody binding intensity, expressed as a percentage of the total number of NIR680-labeled cells, for (A) PI3P ($n = 5$, normal glucose; $n = 4$, hyperglycemia), (B) PI4P ($n = 5$; $n = 4$), (C) PI(3,4)P_2 ($n = 5$; $n = 4$), (D) PI(3,5)P_2 ($n = 5$; $n = 4$), (E) PI(4,5)P_2 ($n = 5$; $n = 4$), and (F) PIP_3 ($n = 5$; $n = 4$) under normal glucose and hyperglycemic conditions. Bars represent mean values; error bars denote ± s.d. from independent measurements. Statistical significance was determined using a two-tailed Student's *t*-test with unequal variance ($P < 0.05$).

Within TNBC Hs578T cell lines, no significant differences in antibody binding were observed between normal glucose and hyperglycemia (Figs. 22A-F).

Fig. 22

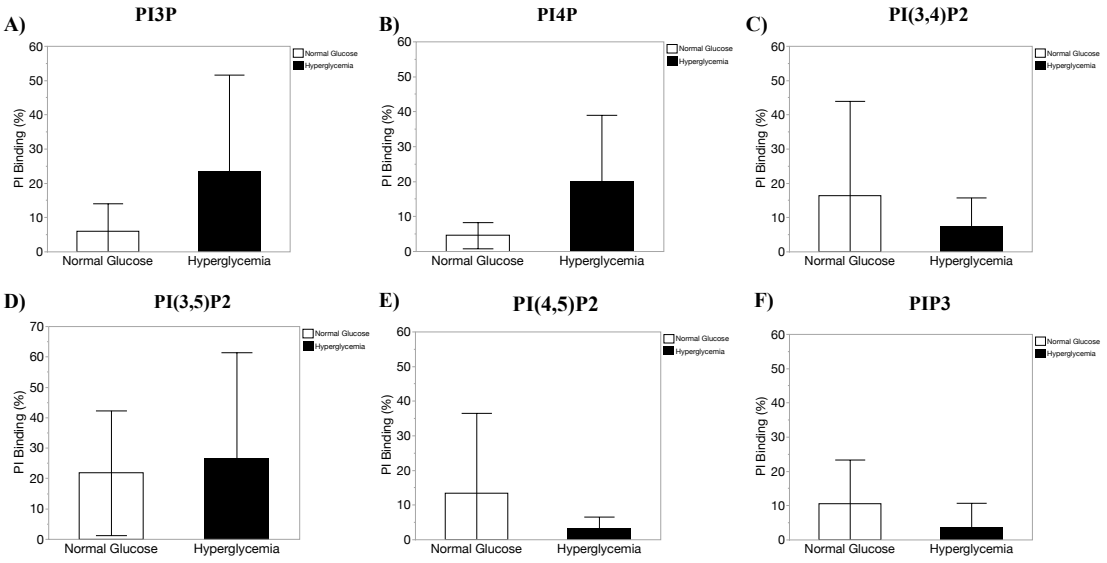

Figure 22 | Hs578T PIP Antibody Binding in Normal Glucose and Hyperglycemia.

Antibody binding intensity, expressed as a percentage of the total number of NIR680-labeled cells, for (A) PI3P ($n = 5$, normal glucose; $n = 5$, hyperglycemia), (B) PI4P ($n = 5$; $n = 5$), (C) PI(3,4)P_2 ($n = 5$; $n = 5$), (D) PI(3,5)P_2 ($n = 5$; $n = 5$), (E) PI(4,5)P_2 ($n = 5$; $n = 5$), and (F) PIP_3 ($n = 5$; $n = 5$) under normal glucose and hyperglycemic conditions. Bars represent mean values; error bars denote ± s.d. from independent measurements. Statistical significance was determined using a two-tailed Student's *t*-test with unequal variance ($P < 0.05$).

Within TNBC MDA-MB-231 cell lines, no significant differences in antibody binding were observed between normal glucose and hyperglycemia (Figs. 23A-F).

Fig. 23

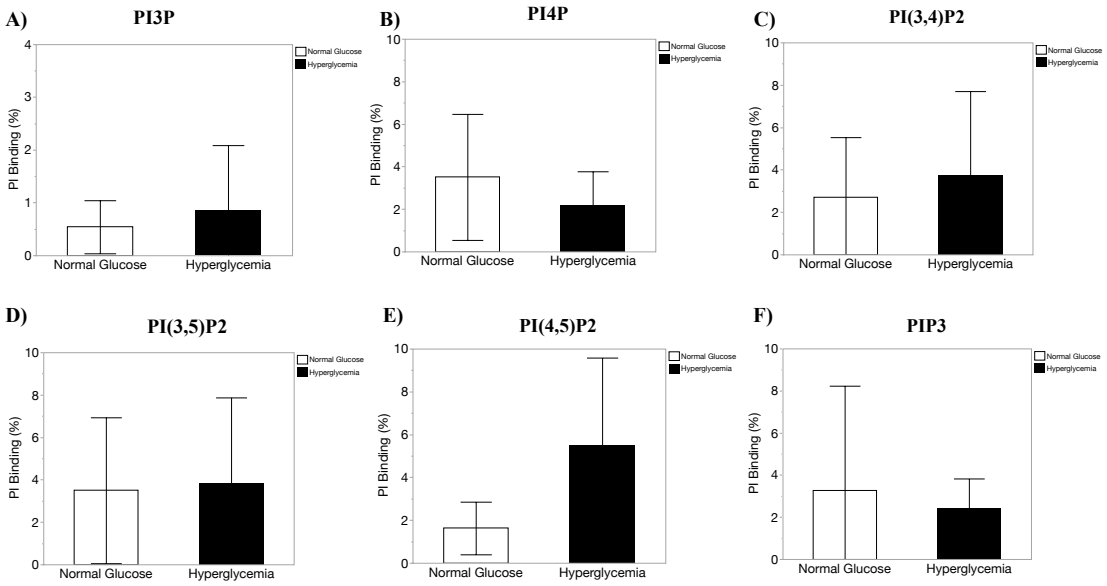

Figure 23 | MDA-MB-231 PIP Antibody Binding in Normal Glucose and Hyperglycemia. Antibody binding intensity, expressed as a percentage of the total number of NIR680-labeled cells, for (A) PI3P ($n = 5$, normal glucose; $n = 5$, hyperglycemia), (B) PI4P ($n = 5$; $n = 5$), (C) $PI(3,4)P_2$ ($n = 5$; $n = 5$), (D) $PI(3,5)P_2$ ($n = 5$; $n = 5$), (E) $PI(4,5)P_2$ ($n = 5$; $n = 5$), and (F) PIP_3 ($n = 5$; $n = 5$) under normal glucose and hyperglycemic conditions. Bars represent mean values; error bars denote ± s.d. from independent measurements. Statistical significance was determined using a two-tailed Student's *t*-test with unequal variance ($P < 0.05$).

Within TNBC MDA-MB-468 cell lines, no significant differences in antibody binding were observed between normal glucose and hyperglycemia (Figs. 24A-F).

Fig. 24

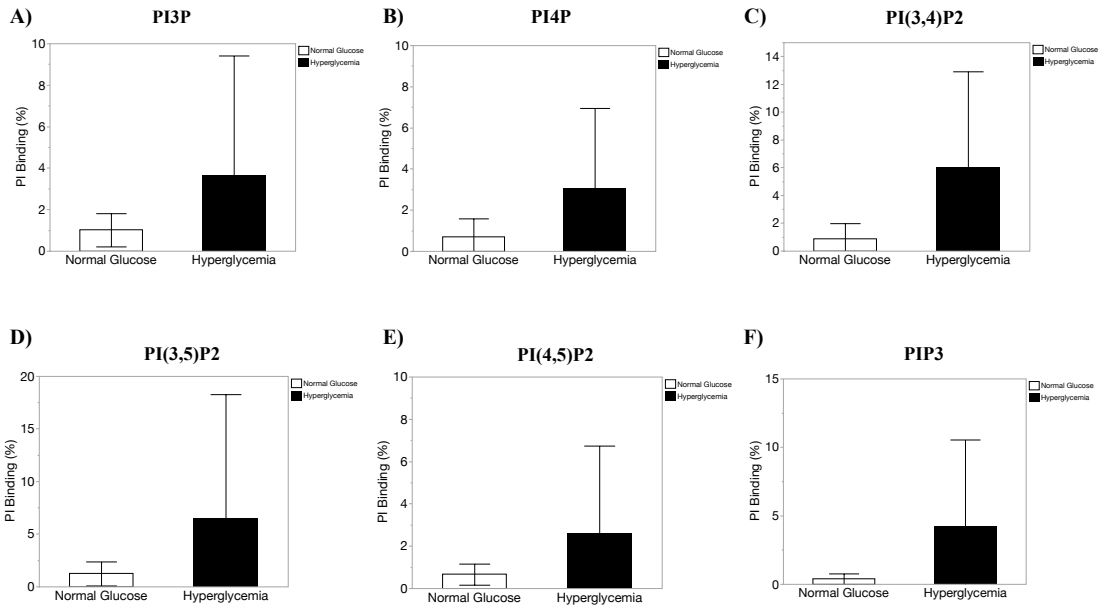

Figure 24 | MDA-MB-468 PIP Antibody Binding in Normal Glucose and Hyperglycemia. Antibody binding intensity, expressed as a percentage of the total number of NIR680-labeled cells, for (A) PI3P ($n = 4$, normal glucose; $n = 5$, hyperglycemia), (B) PI4P ($n = 4$; $n = 5$), (C) $PI(3,4)P_2$ ($n = 4$; $n = 5$), (D) $PI(3,5)P_2$ ($n = 4$; $n = 5$), (E) $PI(4,5)P_2$ ($n = 4$; $n = 5$), and (F) PIP_3 ($n = 4$; $n = 5$) under normal glucose and hyperglycemic conditions. Bars represent mean values; error bars denote ± s.d. from independent measurements. Statistical significance was determined using a two-tailed Student's *t*-test with unequal variance ($P < 0.05$).

Further analysis of PIP binding across cell lines revealed distinct patterns between glucose conditions. Under normoglycemia, no statistically significant differences were observed among any of the cell lines (Figs. 25A–F). In hyperglycemia, however, significant differences emerged, with HEK293T and KTB36 (non-breast cancer lines) showing altered PI4P and PIP_3 binding compared to MDA-MB-231 (Figs. 25B, F).

Additionally, KTB36 displayed a significant difference in PI(4,5)P_2 binding relative to MDA-MB-231 (Fig. 25E).

Fig. 25

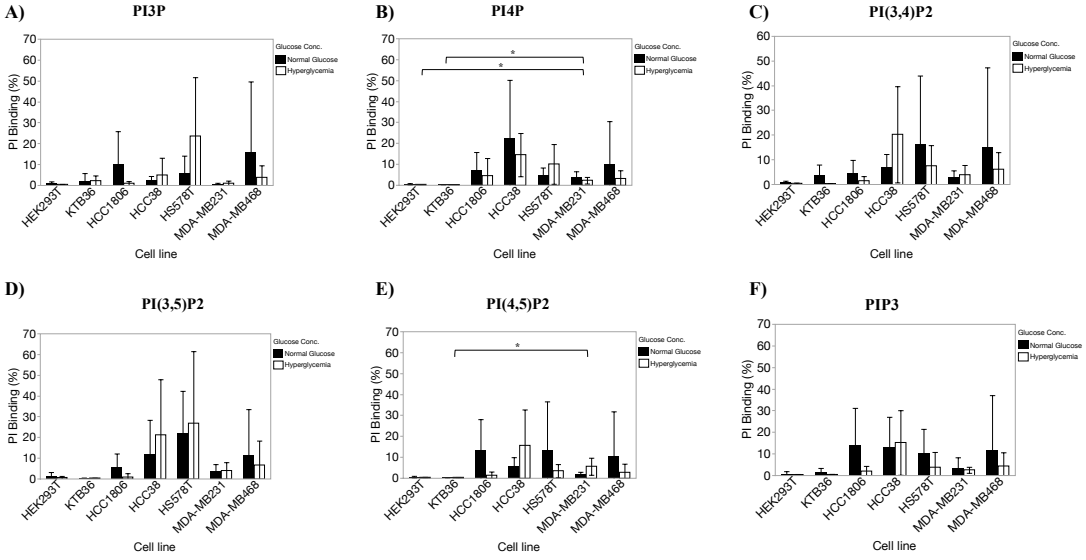

Figure 25 | Phosphatidylinositol Phosphate (PIP) Antibody Binding of TNBC Cell Lines in Normal Glucose and Hyperglycemia. Antibody binding intensity, expressed as a percentage of the total number of NIR680-labeled cells, for (A) PI3P (B) PI4P (C) PI(3,4)P_2 (D) PI(3,5)P_2 (E) PI(4,5)P_2 and (F) PIP_3 under normal glucose and hyperglycemic conditions. Bars represent mean values; error bars denote ± s.e.m. from independent measurements. Statistical significance was assessed using a two-tailed Student's *t*-test with unequal variance ($P < 0.05$).

Although hyperglycemia did not significantly alter PIP surface accessibility within individual cell lines, select PIP species—including PI4P, PI(4,5)P_2, and PIP_3—were able to differentiate non-breast cancer cells from aggressive TNBC under hyperglycemic conditions. This pattern suggests that these lipids could serve as candidate biomarkers for

distinguishing malignant from non-malignant cells in glucose-rich environments, such as those associated with diabetes or tumor microenvironments. Because these PIPs are directly involved in signaling pathways regulating adhesion, cytoskeletal remodeling, and growth, their differential surface accessibility may reflect underlying metabolic and signaling adaptations specific to TNBC cells. Such findings highlight the potential of lipid-based profiling as a complementary approach to traditional protein biomarkers for cancer classification and monitoring. Fold differences between the cell lines across all PIP derivatives are shown in tables 12 - 17 in the appendix.

At the same time, several limitations temper confidence in these observations. The large error margins across replicates increase variability and raise the possibility that the detected differences are less robust than they appear. Furthermore, the absence of viability controls means that dead or ruptured cells could have contributed to apparent antibody binding, particularly for PIP species that are not typically enriched on the outer leaflet of the plasma membrane. This raises the concern that surface labeling of certain PIPs may be, at least in part, an artifact of compromised membrane integrity rather than a true reflection of physiological distribution. Addressing these issues with viability gating and expanded replicate numbers will be critical to validate whether these PIPs can reliably serve as biomarkers in hyperglycemic contexts.

Chapter 4 – Discussion

Triple-negative breast cancer (TNBC) remains one of the most aggressive breast cancer subtypes, defined by its high heterogeneity, lack of targeted therapies, and poor clinical outcomes. Increasing evidence suggests that systemic metabolic dysregulation, particularly hyperglycemia associated with Type 2 diabetes, may exacerbate tumor progression by fueling oncogenic signaling, enhancing proliferation, and promoting survival [59]. These observations have important clinical relevance, as patients with metabolic comorbidities often present with more advanced or treatment-resistant disease. In this study, we investigated whether hyperglycemia promotes aggressive TNBC phenotypes and whether phosphatidylinositol (PI) lipids, central regulators of membrane signaling, could serve as biomarkers of glucose-driven tumor progression.

By combining functional assays of migration, extracellular matrix (ECM) attachment and proliferation with lipidomic profiling of giant plasma membrane vesicles (GPMVs) and live-cell PI antibody screening, we aimed to capture both phenotypic outcomes and underlying molecular mechanisms. This integrative approach provides perspective of how glucose availability influences TNBC aggressiveness and highlights candidate biomarkers that may differentiate TNBC sub-typical cell lines and potentially translate into diagnostic or therapeutic tools.

Trans-well migration, scratch wound, and cell accumulation assays demonstrated that hyperglycemia enhances TNBC aggressiveness, though responses were highly cell line specific. ECM attachment experiments and did not show within cell line differences driven by hyperglycemia. HCC1806 and HCC38 consistently exhibited increased migration under hyperglycemia, suggesting that these subtypes adopt glucose-fueled

migratory programs potentially through enhanced focal adhesion turnover or cytoskeletal remodeling. In contrast, MDA-MB-231 showed suppressed migration under hyperglycemia, indicating that not all TNBCs benefit equally from elevated glucose and that some may redirect metabolic resources toward alternative survival pathways. Scratch wound assays reinforced this heterogeneity, with HCC1806 emerging as the most consistently migratory, while MDA-MB-468 exhibited weak migration despite strong proliferative capacity. These divergent responses underscore the metabolic plasticity of TNBC, where distinct subtypes channel glucose into different oncogenic outputs, migration, proliferation, or stress adaptation—rather than adopting a uniform phenotype.

ECM Attachment assays further emphasized this heterogeneity. Hyperglycemia did not uniformly alter adhesion across TNBCs but instead revealed ECM protein-specific preferences. HCC1806 adhered strongly to collagen under hyperglycemia, consistent with its enhanced migratory phenotype, while HCC38 favored fibronectin, aligning with its intermediate wound closure. Interestingly, MDA-MB-468 adhered robustly to collagen but migrated poorly, suggesting that strong ECM attachment does not necessarily translate into greater motility and may reflect integrin-mediated signaling biased toward survival or proliferation. These findings highlight how differential ECM protein attachment and downstream signaling may interact with metabolic status to shape aggressiveness in distinct TNBC models.

Proliferation assays revealed a more uniform effect of hyperglycemia, with all TNBC cell lines exhibiting enhanced growth consistent with the Warburg effect [40]. However, growth dynamics diverged significantly. Hs578T and MDA-MB-468 expanded rapidly but later declined, possibly due to glucose-induced metabolic stress or cell death. MDA-

MB-231 and HCC1806 maintained steady proliferation without such inflections, suggesting more balanced metabolic adaptations. Notably, MDA-MB-468 demonstrated strong proliferation yet weak migration, implying preferential glucose allocation to biosynthesis over motility. In contrast, Hs578T leveraged glucose for both migration and proliferative phenotypes, reflecting dual exploitation of metabolic inputs. These differences may stem from variable activation of PI3K/AKT/mTOR signaling [46], [52] or $PI(4,5)P_2$-dependent cytoskeletal regulation [60], underscoring the role of lipid signaling in shaping how hyperglycemia is utilized by different TNBC subtypes.

Lipidomic profiling of GPMVs provided molecular context for these functional patterns. While hyperglycemia did not significantly remodel PI abundance within individual lines, inter-line differences were evident. For instance, $PI(3,4)P_2$ levels were reduced in Hs578T, MDA-MB-231, and MDA-MB-468 compared to HCC38, potentially reflecting impaired receptor recycling and altered AKT activation in metastatic-prone lines. Importantly, hyperglycemia appeared to reduce compositional diversity between primary tumor–derived and metastatic lines, suggesting that elevated glucose may converge PI profiles toward a more uniform signaling state. This remodeling could reflect metabolic adaptation that enables progression despite heterogeneity at baseline.

Live-cell PI antibody screening extended these observations by demonstrating that select PI species can differentiate TNBC from non-breast cell lines. Although replicate variability and technical limitations reduced statistical power, certain PIs, particularly PI4P, $PI(4,5)P_2$, and PIP_3, consistently separated TNBC cells from HEK293T and KTB36 under hyperglycemia. These findings align with reports of PIs appearing on the outer leaflet of the plasma membrane, where they can modulate adhesion and signaling [57].

While hyperglycemia did not markedly shift surface PI accessibility within individual cell lines, inter-line comparisons suggest that PIs may act as distinguishing markers of malignant versus non-malignant states, especially in metabolically stressed environments. These results support the concept that hyperglycemia promotes TNBC aggressiveness through heterogeneous, subtype-specific mechanisms, and that PIs represent promising biomarkers of this process. Functional assays revealed that glucose availability can be exploited for proliferation, migration, or adhesion in different TNBC subtypes, while lipidomics and antibody profiling identified PI signatures that distinguish cancerous from non-cancerous cells. Clinically, PI profiling could complement current molecular diagnostics, stratify patients based on aggressiveness, and inform targeted therapies that disrupt PI-mediated pathways. This may be particularly important for patients with comorbid hyperglycemia, where metabolic and signaling crosstalk may accelerate disease progression. Future studies should refine PI detection methods, incorporate viability controls to mitigate confounding from dead cells, and explore how PI-targeted interventions may selectively impair glucose-driven tumor phenotypes.

Chapter 5 – Future Directions

Building on the findings of this study, future work should focus on clarifying the mechanistic basis of TNBC heterogeneity under hyperglycemic conditions and establishing the clinical utility of phosphatidylinositol lipids as biomarkers. The diverse responses of TNBC cell lines to hyperglycemia suggest that underlying genetic backgrounds, including mutations in PI3K, Ras, or BRCA1/2, may strongly shape metabolic adaptation and aggressiveness. Stratifying functional and lipidomic results by genomic alterations, cellular origin (primary versus metastatic), morphological traits, and patient ancestry will be critical to uncover biologically meaningful variability. Such integrative analyses may clarify how systemic glucose dysregulation interacts with tumor-intrinsic features to modulate PIP remodeling and downstream signaling, ultimately influencing TNBC progression.

Refinement of experimental design will also be essential. While the antibody-based PIP detection assay demonstrated potential, variability across replicates and relatively high error margins limited interpretability. Incorporating more sensitive lipidomic techniques and increasing the number of biological replicates will enhance reproducibility and statistical power. Expanding the panel of comparator cell lines to include $HER2^+$ and HR^+ breast cancers, as well as additional non-breast epithelial models of diverse genetic backgrounds, will broaden biological relevance and determine whether PIP remodeling represents a unique hallmark of TNBC or a broader feature of malignancy. Moreover, extending assays to include PIP derivatives not typically localized to the outer leaflet of the plasma membrane could yield new insights into non-canonical signaling roles for these lipids.

Future work should also move beyond in vitro measures of proliferation, migration, and adhesion to assess whether glucose-dependent phenotypes translate into metastatic colonization of secondary tissues such as lung, bone, liver, and brain. Brain metastasis, in particular, remains a devastating clinical outcome for TNBC patients yet was not directly addressed in this study. Incorporating in vivo models will provide critical evidence for whether hyperglycemia modulates metastatic tropism and whether PIP-based signatures persist in secondary tumor sites. Nanoparticle-based platforms, such as silver-coated lipid nanoparticles conjugated to PIP antibodies, represent an intriguing strategy to track PIP dynamics in real time within metastatic microenvironments.

Finally, mapping the regulatory networks underlying PIP remodeling will help determine whether observed shifts are causal drivers of TNBC aggressiveness or secondary consequences of metabolic adaptation. Parallel quantification of both phosphorylated and unphosphorylated PI species under normal glucose and hyperglycemic conditions, alongside upstream regulators such as PI kinases and phosphatases, will clarify whether hyperglycemia-induced lipidomic changes reflect altered enzymatic activity, redistribution of lipid pools, or remodeling of membrane microdomains. Establishing these mechanistic links will be necessary to translate PIPs into clinically actionable biomarkers.

In summary, future research should adopt a multi-layered approach that integrates genomic profiling, advanced lipidomics, and metastatic models to validate PIPs as robust indicators of TNBC aggressiveness. Such work will provide deeper insight into how systemic metabolic dysregulation contributes to tumor progression and may ultimately

enable the development of biomarker-driven strategies for early detection, patient stratification, and targeted therapy in hyperglycemia-associated TNBC.

Appendices

Appendix A: Fold Difference Table for Transwell Migration Experiment.

Table 1

Fold Differences		
Cell lines	**Normal Glucose**	**Hyperglycemia**
HCC1806 vs HCC38	0.690598928	1.277552706
HC1806 vs Hs578T	0.857732362	1.164629684
HCC1806 vs MDA-MB231	1.409797604	3.47301451
HCC38 vs Hs578T	1.242012299	0.911609891
HCC38 vs MDA-MB231	2.041412964	2.718490199
Hs578T vs MDA-MB231	1.643633454	2.982076242

Table 1 | Table Showing Fold Differences in Transwell Migration of Aggressive TNBC Cell Lines Under Normal Glucose and Hyperglycemic Conditions. Migration was quantified after overnight incubation in the indicated glucose conditions. Values greater than 1 indicate upregulation while values lower than 1 indicate down regulation.

Appendix B: Fold Difference Table for Scratch Wound Migration Experiment.

Table 2

Fold Differences		
Cell lines	**Normal Glucose**	**Hyperglycemia**
HCC1806 vs HCC38	2.436917416	5.959079284
HCC1806 vs Hs578T	1.183617951	0.772091311
HCC1806 vs MDA-MB-231	1.003620016	0.799702543
HCC1806 vs MDA-MB-468	3.44310305	2.709827486
HCC38 vs Hs578T	0.485702939	0.129565538
HCC38 vs MDA-MB-231	0.411839978	0.13419901
HCC38 vs MDA-MB-468	1.412892791	0.454739291
Hs578T vs MDA-MB-231	0.847925647	1.035761615
Hs578T vs MDA-MB-468	2.90896488	3.509724107
MDA-MB-231 vs MDA-MB-468	3.430683919	3.388544292

Table 2 | Table Showing Fold Differences in Wound Closure in 24 Hours of Aggressive TNBC Cell Lines Under Normal Glucose and Hyperglycemic Conditions. Values greater than 1 indicate upregulation while values lower than 1 indicate down regulation.

Appendix C: Fold Difference Tables for ECM Attachment Experiments.

Table 3

Fold Differences		
Cell lines	**Normal Glucose**	**Hyperglycemia**
HCC1806 vs HCC38	1.5887674	1.885087886
HCC1806 vs Hs578T	1.034201657	1.255203762
HCC1806 vs MDA-MB-231	0.656948574	1.097599305
HCC1806 vs MDA-MB-468	0.568578342	0.948492879
HCC38 vs Hs578T	0.65094592	0.665859545
HCC38 vs MDA-MB-231	0.413495754	0.582253652
HCC38 vs MDA-MB-468	0.357873872	0.503155787
Hs578T vs MDA-MB-231	0.635222898	0.874439146
Hs578T vs MDA-MB-468	0.549775121	0.755648532
MDA-MB-231 vs MDA-MB-468	0.86548379	0.864152223

Table 3 | Table Showing Fold Differences in Collagen Attachment of TNBC Cell Lines Under Normal Glucose and Hyperglycemic Conditions. Values greater than 1 indicate upregulation while values lower than 1 indicate downregulation.

Table 4

Fold Differences		
Cell lines	**Normal Glucose**	**Hyperglycemia**
HCC1806 vs HCC38	1.006738724	2.768081626
HCC1806 vs Hs578T	1.681551944	1.567432745
HCC1806 vs MDA-MB-231	0.753883876	7.21672022
HCC1806 vs MDA-MB-468	0.421319273	14.05072813
HCC38 vs Hs578T	1.670296279	0.566252357
HCC38 vs MDA-MB-231	0.748837666	2.607119729
HCC38 vs MDA-MB-468	0.418499123	5.075980419
Hs578T vs MDA-MB-231	0.44832625	4.604165788
Hs578T vs MDA-MB-468	0.250553826	8.964166519
MDA-MB-231 vs MDA-MB-468	0.558864948	1.946968665

Table 4 | Table Showing Fold Differences in Fibronectin Attachment of TNBC Cell Lines Under Normal Glucose and Hyperglycemic Conditions. Values greater than 1 indicate upregulation while values lower than 1 indicate downregulation.

Appendix D: Fold Difference table for Cell Accumulation Experiment.

Table 5

Fold Differences			
Cell lines	**Time (Days)**	**Normal Glucose**	**Hyperglycemia**
HCC1806 vs Hs578T	0	1	1
HCC1806 vs Hs578T	1	0.58136679	0.328746382
HCC1806 vs Hs578T	2	0.602696429	0.38868999
HCC1806 vs Hs578T	3	0.306565812	0.319464201
HCC1806 vs Hs578T	4	0.318131731	0.272186094
HCC1806 vs Hs578T	5	0.517130656	#VALUE!
HCC1806 vs Hs578T	6	0.170709707	#VALUE!
HCC1806 vs MDA-MB-231	0	1	1
HCC1806 vs MDA-MB-231	1	0.965192348	0.512732538
HCC1806 vs MDA-MB-231	2	0.862028419	0.628363132
HCC1806 vs MDA-MB-231	3	0.628204517	0.907213283
HCC1806 vs MDA-MB-231	4	0.755054783	0.398051427
HCC1806 vs MDA-MB-231	5	0.532592081	0.350085681
HCC1806 vs MDA-MB-231	6	0.78230311	#VALUE!
HCC1806 vs MDA-MB-468	0	1	1
HCC1806 vs MDA-MB-468	1	0.618992351	0.436449756
HCC1806 vs MDA-MB-468	2	0.430720164	0.509119346
HCC1806 vs MDA-MB-468	3	0.41577264	0.627138575
HCC1806 vs MDA-MB-468	4	0.314583495	0.214608127
HCC1806 vs MDA-MB-468	5	0.412860912	0.13151726
HCC1806 vs MDA-MB-468	6	0.120424662	#VALUE!
Hs578T vs MDA-MB-231	0	1	1
Hs578T vs MDA-MB-231	1	1.66021239	1.559659866
Hs578T vs MDA-MB-231	2	1.430286255	1.616617738
Hs578T vs MDA-MB-231	3	2.049166909	2.839796386
Hs578T vs MDA-MB-231	4	2.373402931	1.627638291
Hs578T vs MDA-MB-231	5	1.029898488	#VALUE!
Hs578T vs MDA-MB-231	6	4.582651593	0.618366667
Hs578T vs MDA-MB-468	0	1	1
Hs578T vs MDA-MB-468	1	1.064719144	1.32761843
Hs578T vs MDA-MB-468	2	0.714655244	1.309833953
Hs578T vs MDA-MB-468	3	1.356226375	1.963094999
Hs578T vs MDA-MB-468	4	0.988846647	0.87753587
Hs578T vs MDA-MB-468	5	0.798368665	#VALUE!
Hs578T vs MDA-MB-468	6	0.705435351	0.610028088
MDA-MB-231 vs MDA-MB-468	0	1	1
MDA-MB-231 vs MDA-MB-468	1	0.641315021	0.851223052
MDA-MB-231 vs MDA-MB-468	2	0.499658891	0.81023109
MDA-MB-231 vs MDA-MB-468	3	0.661842805	0.691280195
MDA-MB-231 vs MDA-MB-468	4	0.41663665	0.539146735
MDA-MB-231 vs MDA-MB-468	5	0.775191608	0.375671634
MDA-MB-231 vs MDA-MB-468	6	0.153936064	0.986515154

Table 5 | Table Showing Fold Differences in Cell Accumulation of Aggressive TNBC Cell Lines Under Normal Glucose and Hyperglycemic Conditions Across Each Day. Accumulation was quantified over 5 days and normalized against day 0. Values greater than 1 indicate upregulation while values lower than 1 indicate down regulation.

Appendix E: Fold Difference Tables for Giant Plasma Membrane Vesicle Experiment.

Table 6

Fold Differences			
Cell lines	**PI**	**Normal Glucose**	**Hyperglycemia**
HCC38 vs Hs578T	PI3P	0.84125142	0.803793481
HCC38 vs MDA-MB-231	PI3P	0.934687402	0.909303539
HCC38 vs MDA-MB-468	PI3P	0.972929991	0.87487066
Hs578T vs MDA-MB-231	PI3P	1.111067844	1.131265133
Hs578T vs MDA-MB-468	PI3P	1.156527011	1.088427166
MDA-MB-231 vs MDA-MB-468	PI3P	1.040914844	0.96213269

Table 6 | Table Showing Fold Differences in PI3P Accumulation in Giant Plasma Membrane Vesicles (GPMV) in TNBC Cell Lines Under Normal Glucose and Hyperglycemic Conditions. Values greater than 1 indicate upregulation while values lower than 1 indicate down regulation.

Table 7

Fold Differences			
Cell lines	**PI**	**Normal Glucose**	**Hyperglycemia**
HCC38 vs Hs578T	PI4P	0.84301724	0.882345929
HCC38 vs MDA-MB-231	PI4P	0.841196758	0.934170049
HCC38 vs MDA-MB-468	PI4P	0.789058108	0.87748927
Hs578T vs MDA-MB-231	PI4P	0.997840517	1.05873447
Hs578T vs MDA-MB-468	PI4P	0.935992849	0.994495743
MDA-MB-231 vs MDA-MB-468	PI4P	0.938018484	0.994495743

Table 7 | Table Showing Fold Differences in PI4P Accumulation in Giant Plasma Membrane Vesicles (GPMV) in TNBC Cell Lines Under Normal Glucose and Hyperglycemic Conditions. Values greater than 1 indicate upregulation while values lower than 1 indicate down regulation.

Table 8

Fold Differences			
Cell lines	**PI**	**Normal Glucose**	**Hyperglycemia**
HCC38 vs Hs578T	PI3,4P2	2.292935082	1.850709893
HCC38 vs MDA-MB-231	PI3,4P2	1.535119981	1.260460238
HCC38 vs MDA-MB-468	PI3,4P2	1.706016657	1.683617728
Hs578T vs MDA-MB-231	PI3,4P2	0.669499976	0.681068514
Hs578T vs MDA-MB-468	PI3,4P2	0.744031818	0.909714556
MDA-MB-231 vs MDA-MB-468	PI3,4P2	1.111324638	1.335716652

Table 8 | Table Showing Fold Differences in PI(3,4)P2 Accumulation in Giant Plasma Membrane Vesicles (GPMV) in TNBC Cell Lines Under Normal Glucose and Hyperglycemic Conditions. Values greater than 1 indicate upregulation while values lower than 1 indicate down regulation.

Table 9

Fold Differences			
Cell lines	**PI**	**Normal Glucose**	**Hyperglycemia**
HCC38 vs Hs578T	PI3,5P2	0.868104041	0.881552189
HCC38 vs MDA-MB-231	PI3,5P2	0.951798901	0.949423149
HCC38 vs MDA-MB-468	PI3,5P2	0.985891824	0.930583352
Hs578T vs MDA-MB-231	PI3,5P2	1.096411094	1.076990291
Hs578T vs MDA-MB-468	PI3,5P2	1.135683947	1.055619126
MDA-MB-231 vs MDA-MB-468	PI3,5P2	1.03581946	0.980156586

Table 9 | Table Showing Fold Differences in PI(3,5)P2 Accumulation in Giant Plasma Membrane Vesicles (GPMV) in TNBC Cell Lines Under Normal Glucose and Hyperglycemic Conditions. Values greater than 1 indicate upregulation while values lower than 1 indicate down regulation.

Table 10

Fold Differences			
Cell lines	**PI**	**Normal Glucose**	**Hyperglycemia**
HCC38 vs Hs578T	PI4,5P2	0.93098451	0.942266154
HCC38 vs MDA-MB-231	PI4,5P2	0.954728402	0.96384267
HCC38 vs MDA-MB-468	PI4,5P2	0.96540826	0.953759192
Hs578T vs MDA-MB-231	PI4,5P2	1.025504069	1.022898537
Hs578T vs MDA-MB-468	PI4,5P2	1.036975643	1.012197231
MDA-MB-231 vs MDA-MB-468	PI4,5P2	1.011186278	0.989538253

Table 10 | Table Showing Fold Differences in PI(4,5)P2 Accumulation in Giant Plasma Membrane Vesicles (GPMV) in TNBC Cell Lines Under Normal Glucose and Hyperglycemic Conditions. Values greater than 1 indicate upregulation while values lower than 1 indicate down regulation.

Table 11

Fold Differences			
Cell lines	**PI**	**Normal Glucose**	**Hyperglycemia**
HCC38 vs Hs578T	PIP3	0.961479695	1.030909362
HCC38 vs MDA-MB-231	PIP3	0.959992251	0.993437184
HCC38 vs MDA-MB-468	PIP3	0.940781596	0.98613341
Hs578T vs MDA-MB-231	PIP3	0.998452964	0.963651336
Hs578T vs MDA-MB-468	PIP3	0.978472662	0.956566549
MDA-MB-231 vs MDA-MB-468	PIP3	0.97998874	0.992647977

Table 11 | Table Showing Fold Differences in PIP3 Accumulation in Giant Plasma Membrane Vesicles (GPMV) in TNBC Cell Lines Under Normal Glucose and Hyperglycemic Conditions. Values greater than 1 indicate upregulation while values lower than 1 indicate down regulation.

Appendix F: Fold Difference tables for Live Cell Antibody Biomarker Screen Experiment.

Table 12

Fold Differences			
Cell lines	**PI**	**Normal Glucose**	**Hyperglycemia**
HEK293T vs KTB36	PI3P	0.368265003	0.144365397
HEK293T vs HCC1806	PI3P	0.073519021	0.355803365
HEK293T vs HCC38	PI3P	0.318944761	0.062475704
HEK293T vs Hs578T	PI3P	0.127467323	0.010633404
HEK293T vs MDA-MB-231	PI3P	1.384530936	0.351309304
HEK293T vs MDA-MB-468	PI3P	0.046656134	0.081821287
KTB36 vs HCC1806	PI3P	0.199636188	2.464602831
KTB36 vs HCC38	PI3P	0.866074045	0.432760935
KTB36 vs Hs578T	PI3P	0.34612934	0.073656184
KTB36 vs MDA-MB-231	PI3P	3.759604967	2.433473066
KTB36 vs MDA-MB-468	PI3P	0.126691741	0.566765228
HCC1806 vs HCC38	PI3P	4.338261787	0.175590537
HCC1806 vs Hs578T	PI3P	1.733800588	0.02988562
HCC1806 vs MDA-MB-231	PI3P	18.83228189	0.987369257
HCC1806 vs MDA-MB-468	PI3P	0.634613103	0.229962094
HCC38 vs Hs578T	PI3P	0.399653288	0.170200631
HCC38 vs MDA-MB-231	PI3P	4.340974062	5.623134782
HCC38 vs MDA-MB-468	PI3P	0.146282805	1.309649698
Hs578T vs MDA-MB-231	PI3P	10.86184998	33.03827222
Hs578T vs MDA-MB-468	PI3P	0.366024275	7.694740552
MDA-MB-231 vs MDA-MB-468	PI3P	0.033698152	0.232903843

Table 12 | Table Showing Fold Differences in PI3P Antibody Binding in Non-Breast Cancer and TNBC Cell Lines Under Normal Glucose and Hyperglycemic Conditions. Values greater than 1 indicate upregulation while values lower than 1 indicate down regulation.

Table 13

Fold Differences			
Cell lines	**PI**	**Normal Glucose**	**Hyperglycemia**
HEK293T vs KTB36	PI4P	2.931931182	2.290706715
HEK293T vs HCC1806	PI4P	0.050686186	0.050636969
HEK293T vs HCC38	PI4P	0.016438614	0.003930667
HEK293T vs Hs578T	PI4P	0.080850581	0.005337712
HEK293T vs MDA-MB-231	PI4P	0.104273081	0.101536782
HEK293T vs MDA-MB-468	PI4P	0.037016415	0.073203246
KTB36 vs HCC1806	PI4P	0.017287645	0.022105392
KTB36 vs HCC38	PI4P	0.005606753	0.001715919
KTB36 vs Hs578T	PI4P	0.027575879	0.00233016
KTB36 vs MDA-MB-231	PI4P	0.035564641	0.044325527
KTB36 vs MDA-MB-468	PI4P	0.012625267	0.031956621
HCC1806 vs HCC38	PI4P	0.324321383	0.077624447
HCC1806 vs Hs578T	PI4P	1.595120638	0.105411366
HCC1806 vs MDA-MB-231	PI4P	2.057228807	2.005190754
HCC1806 vs MDA-MB-468	PI4P	0.730305796	1.445648257
HCC38 vs Hs578T	PI4P	4.91833323	1.357966076
HCC38 vs MDA-MB-231	PI4P	6.343179673	25.83194896
HCC38 vs MDA-MB-468	PI4P	2.251796621	18.62362068
Hs578T vs MDA-MB-231	PI4P	1.289701079	19.02252893
Hs578T vs MDA-MB-468	PI4P	0.457837344	13.71434899
MDA-MB-231 vs MDA-MB-468	PI4P	0.35499493	0.720952984

Table 13 | Table Showing Fold Differences in PI4P Antibody Binding in Non-Breast Cancer and TNBC Cell Lines Under Normal Glucose and Hyperglycemic Conditions. Values greater than 1 indicate upregulation while values lower than 1 indicate down regulation.

Table 14

Fold Differences			
Cell lines	**PI**	**Normal Glucose**	**Hyperglycemia**
HEK293T vs KTB36	PI(3,4)P2	0.190056041	1.561079831
HEK293T vs HCC1806	PI(3,4)P2	0.152596773	0.20592825
HEK293T vs HCC38	PI(3,4)P2	0.098343636	0.006829594
HEK293T vs Hs578T	PI(3,4)P2	0.041772841	0.037253605
HEK293T vs MDA-MB-231	PI(3,4)P2	2.691075122	3.762933364
HEK293T vs MDA-MB-468	PI(3,4)P2	15.18388008	5.988647525
KTB36 vs HCC1806	PI(3,4)P2	0.802904094	0.131913978
KTB36 vs HCC38	PI(3,4)P2	0.517445463	0.004374917
KTB36 vs Hs578T	PI(3,4)P2	0.219792231	0.023863998
KTB36 vs MDA-MB-231	PI(3,4)P2	1.327229926	0.046844743
KTB36 vs MDA-MB-468	PI(3,4)P2	0.235228112	0.029434634
HCC1806 vs HCC38	PI(3,4)P2	0.644467336	0.033164921
HCC1806 vs Hs578T	PI(3,4)P2	0.273746556	0.180905754
HCC1806 vs MDA-MB-231	PI(3,4)P2	2.691075122	3.762933364
HCC1806 vs MDA-MB-468	PI(3,4)P2	0.292971618	0.223135061
HCC38 vs Hs578T	PI(3,4)P2	0.424764051	5.454731982
HCC38 vs MDA-MB-231	PI(3,4)P2	2.56496582	10.70757381
HCC38 vs MDA-MB-468	PI(3,4)P2	0.454594983	6.728044449
Hs578T vs MDA-MB-231	PI(3,4)P2	6.038566154	1.962988071
Hs578T vs MDA-MB-468	PI(3,4)P2	1.070229419	1.233432636
MDA-MB-231 vs MDA-MB-468	PI(3,4)P2	0.177232375	0.628344438

Table 14 | Table Showing Fold Differences in PI(3,4)P2 Antibody Binding in Non-Breast Cancer and TNBC Cell Lines Under Normal Glucose and Hyperglycemic Conditions. Values greater than 1 indicate upregulation while values lower than 1 indicate down regulation.

Table 15

Fold Differences			
Cell lines	**PI**	**Normal Glucose**	**Hyperglycemia**
HEK293T vs KTB36	PI(3,5)P2	4.544070568	2.212960398
HEK293T vs HCC1806	PI(3,5)P2	0.216833921	0.708376661
HEK293T vs HCC38	PI(3,5)P2	0.098586797	0.012688673
HEK293T vs Hs578T	PI(3,5)P2	0.054513889	0.018708067
HEK293T vs MDA-MB-231	PI(3,5)P2	0.339276444	0.129844071
HEK293T vs MDA-MB-468	PI(3,5)P2	0.106004745	0.076715725
KTB36 vs HCC1806	PI(3,5)P2	0.047717992	0.320103632
KTB36 vs HCC38	PI(3,5)P2	0.021695701	0.0057338
KTB36 vs Hs578T	PI(3,5)P2	0.011996708	0.008453864
KTB36 vs MDA-MB-231	PI(3,5)P2	0.074663551	0.058674376
KTB36 vs MDA-MB-468	PI(3,5)P2	0.023328147	0.03466656
HCC1806 vs HCC38	PI(3,5)P2	0.454665011	0.017912324
HCC1806 vs Hs578T	PI(3,5)P2	0.251408491	0.026409773
HCC1806 vs MDA-MB-231	PI(3,5)P2	1.564683435	0.183298065
HCC1806 vs MDA-MB-468	PI(3,5)P2	0.488875285	0.108297929
HCC38 vs Hs578T	PI(3,5)P2	0.55295324	1.474391187
HCC38 vs MDA-MB-231	PI(3,5)P2	3.441398387	10.23306976
HCC38 vs MDA-MB-468	PI(3,5)P2	1.075242812	6.046000875
Hs578T vs MDA-MB-231	PI(3,5)P2	6.223669812	6.940539153
Hs578T vs MDA-MB-468	PI(3,5)P2	1.94454564	4.100676217
MDA-MB-231 vs MDA-MB-468	PI(3,5)P2	0.312443574	0.590829635

Table 15 | Table Showing Fold Differences in PI(3,5)P2 Antibody Binding in Non-Breast Cancer and TNBC Cell Lines Under Normal Glucose and Hyperglycemic Conditions. Values greater than 1 indicate upregulation while values lower than 1 indicate down regulation.

Table 16

Fold Differences			
Cell lines	**PI**	**Normal Glucose**	**Hyperglycemia**
HEK293T vs KTB36	PI(4,5)P2	2.437062139	1.074460139
HEK293T vs HCC1806	PI(4,5)P2	0.033219608	0.194795544
HEK293T vs HCC38	PI(4,5)P2	0.080826615	0.015317927
HEK293T vs Hs578T	PI(4,5)P2	0.033056929	0.070020732
HEK293T vs MDA-MB-231	PI(4,5)P2	0.270759265	0.043084833
HEK293T vs MDA-MB-468	PI(4,5)P2	0.042813451	0.090576718
KTB36 vs HCC1806	PI(4,5)P2	0.013631006	0.181296204
KTB36 vs HCC38	PI(4,5)P2	0.033165595	0.014256394
KTB36 vs Hs578T	PI(4,5)P2	0.013564254	0.065168292
KTB36 vs MDA-MB-231	PI(4,5)P2	0.111100682	0.040099052
KTB36 vs MDA-MB-468	PI(4,5)P2	0.017567649	0.084299747
HCC1806 vs HCC38	PI(4,5)P2	2.43309962	0.078635919
HCC1806 vs Hs578T	PI(4,5)P2	0.995102942	0.359457564
HCC1806 vs MDA-MB-231	PI(4,5)P2	8.150585855	0.221179768
HCC1806 vs MDA-MB-468	PI(4,5)P2	1.28880063	0.464983519
HCC38 vs Hs578T	PI(4,5)P2	0.408985696	4.571162496
HCC38 vs MDA-MB-231	PI(4,5)P2	3.349877576	2.812706593
HCC38 vs MDA-MB-468	PI(4,5)P2	0.52969497	5.913118638
Hs578T vs MDA-MB-231	PI(4,5)P2	8.190696166	0.615315381
Hs578T vs MDA-MB-468	PI(4,5)P2	1.29514302	1.293569993
MDA-MB-231 vs MDA-MB-468	PI(4,5)P2	0.15812368	2.102287758

Table 16 | Table Showing Fold Differences in PI(4,5)P2 Antibody Binding in Non-Breast Cancer and TNBC Cell Lines Under Normal Glucose and Hyperglycemic Conditions. Values greater than 1 indicate upregulation while values lower than 1 indicate down regulation.

Table 17

Fold Differences			
Cell lines	**PI**	**Normal Glucose**	**Hyperglycemia**
HEK293T vs KTB36	PIP3	0.513822536	0.87718026
HEK293T vs HCC1806	PIP3	0.053176343	0.130431358
HEK293T vs HCC38	PIP3	0.056994595	0.015933799
HEK293T vs Hs578T	PIP3	0.071570487	0.010889232
HEK293T vs MDA-MB-231	PIP3	0.229436171	0.09877397
HEK293T vs MDA-MB-468	PIP3	0.063845081	0.057253389
KTB36 vs HCC1806	PIP3	0.103491653	0.148693904
KTB36 vs HCC38	PIP3	0.110922724	0.018164794
KTB36 vs Hs578T	PIP3	0.139290284	0.012413904
KTB36 vs MDA-MB-231	PIP3	0.446528043	0.112603959
KTB36 vs MDA-MB-468	PIP3	0.124255121	0.06526981
HCC1806 vs HCC38	PIP3	1.071803582	0.122162333
HCC1806 vs Hs578T	PIP3	1.345908397	0.083486302
HCC1806 vs MDA-MB-231	PIP3	4.314628584	0.757286992
HCC1806 vs MDA-MB-468	PIP3	1.200629398	0.438954174
HCC38 vs Hs578T	PIP3	1.255741648	0.683404615
HCC38 vs MDA-MB-231	PIP3	4.025577686	6.199022017
HCC38 vs MDA-MB-468	PIP3	1.120195358	3.593203925
Hs578T vs MDA-MB-231	PIP3	3.205737176	9.070793322
Hs578T vs MDA-MB-468	PIP3	0.892058776	5.257798742
MDA-MB-231 vs MDA-MB-468	PIP3	0.278269467	0.579640452

Table 17 | Table Showing Fold Differences in PIP3 Antibody Binding in Non-Breast Cancer and TNBC Cell Lines Under Normal Glucose and Hyperglycemic Conditions. Values greater than 1 indicate upregulation while values lower than 1 indicate down regulation.

References

"Glucose Metabolism in Cancer: The Warburg Effect and Beyond," in *Advances in Experimental Medicine and Biology*, Cham: Springer International Publishing, 2021, pp. 3–15. doi: 10.1007/978-3-030-65768-0_1.

"Subtypes of Breast Cancer," in *Breast Cancer*, Exon Publications, 2022, pp. 31–42. doi: 10.36255/exon-publications-breast-cancer-subtypes.

N. Afifi and C. A. Barrero, "Understanding Breast Cancer Aggressiveness and Its Implications in Diagnosis and Treatment," *J. Clin. Med.*, vol. 12, no. 4, p. 1375, Feb. 2023, doi: 10.3390/jcm12041375.

E. Ahmad, S. Lim, R. Lamptey, D. R. Webb, and M. J. Davies, "Type 2 diabetes," *The Lancet*, vol. 400, no. 10365, pp. 1803–1820, Nov. 2022, doi: 10.1016/s0140-6736(22)01655-5.

M. Akram, M. Iqbal, M. Daniyal, and A. U. Khan, "Awareness and current knowledge of breast cancer," *Biol. Res.*, vol. 50, no. 1, Dec. 2017, doi: 10.1186/s40659-017-0140-9.

M. A. Ali, K. Czene, L. Eriksson, P. Hall, and K. Humphreys, "Breast Tissue Organisation and its Association with Breast Cancer Risk," *Breast Cancer Res.*, vol. 19, no. 1, p. 103, Dec. 2017, doi: 10.1186/s13058-017-0894-6.

T. Balla, "Phosphoinositides: Tiny Lipids With Giant Impact on Cell Regulation," *Physiol. Rev.*, vol. 93, no. 3, pp. 1019–1137, July 2013, doi: 10.1152/physrev.00028.2012.

A. Bardia *et al.*, “Biomarker analyses in the phase III ASCENT study of sacituzumab govitecan versus chemotherapy in patients with metastatic triple-negative breast cancer,” *Ann. Oncol.*, vol. 32, no. 9, pp. 1148–1156, Sept. 2021, doi: 10.1016/j.annonc.2021.06.002.

B. Bilanges, Y. Posor, and B. Vanhaesebroeck, “PI3K isoforms in cell signalling and vesicle trafficking,” *Nat. Rev. Mol. Cell Biol.*, vol. 20, no. 9, pp. 515–534, Sept. 2019, doi: 10.1038/s41580-019-0129-z.

I. M. Browne, F. André, S. Chandarlapaty, L. A. Carey, and N. C. Turner, “Optimal targeting of PI3K-AKT and mTOR in advanced oestrogen receptor-positive breast cancer,” *Lancet Oncol.*, vol. 25, no. 4, pp. e139–e151, Apr. 2024, doi: 10.1016/s1470-2045(23)00676-9.

T. D. Bunney and M. Katan, “Phosphoinositide signalling in cancer: beyond PI3K and PTEN,” *Nat. Rev. Cancer*, vol. 10, no. 5, pp. 342–352, May 2010, doi: 10.1038/nrc2842.

L. Cantini *et al.*, “Neoadjuvant therapy in hormone Receptor-Positive/HER2-Negative breast cancer,” *Cancer Treat. Rev.*, vol. 123, p. 102669, Feb. 2024, doi: 10.1016/j.ctrv.2023.102669.

W. Cao, R. Wu, G. Cao, and Z. He, “A Comprehensive Review of Computer-Aided Diagnosis of Pulmonary Nodules Based on Computed Tomography Scans,” *IEEE Access*, vol. 8, pp. 154007–154023, 2020, doi: 10.1109/access.2020.3018666.

A. Carbone, “Cancer Classification at the Crossroads,” *Cancers*, vol. 12, no. 4, p. 980, Apr. 2020, doi: 10.3390/cancers12040980.

C. H. Chau, P. S. Steeg, and W. D. Figg, “Antibody–drug conjugates for cancer,” *The Lancet*, vol. 394, no. 10200, pp. 793–804, Aug. 2019, doi: 10.1016/s0140-6736(19)31774-x.

N. Cho, “Molecular subtypes and imaging phenotypes of breast cancer,” *Ultrasonography*, vol. 35, no. 4, pp. 281–288, Oct. 2016, doi: 10.14366/usg.16030.

R. J. Clarke, K. R. Hossain, and K. Cao, “Physiological roles of transverse lipid asymmetry of animal membranes,” *Biochim. Biophys. Acta BBA - Biomembr.*, vol. 1862, no. 10, p. 183382, Oct. 2020, doi: 10.1016/j.bbamem.2020.183382.

J. T. Coates *et al.*, “Parallel Genomic Alterations of Antigen and Payload Targets Mediate Polyclonal Acquired Clinical Resistance to Sacituzumab Govitecan in Triple-Negative Breast Cancer,” *Cancer Discov.*, vol. 11, no. 10, pp. 2436–2445, Oct. 2021, doi: 10.1158/2159-8290.cd-21-0702.

G. Curigliano *et al.*, “Understanding breast cancer complexity to improve patient outcomes: The St Gallen International Consensus Conference for the Primary Therapy of Individuals with Early Breast Cancer 2023,” *Ann. Oncol.*, vol. 34, no. 11, pp. 970–986, Nov. 2023, doi: 10.1016/j.annonc.2023.08.017.

N. Devanathan, S. Jones, G. Kaur, and A. C. Kimble-Hill, “Using Phosphatidylinositol Phosphorylation as Markers for Hyperglycemic Related Breast Cancer,” *Int. J. Mol. Sci.*, vol. 21, no. 7, p. 2320, Mar. 2020, doi: 10.3390/ijms21072320.

G. Di Paolo and P. De Camilli, “Phosphoinositides in cell regulation and membrane dynamics,” *Nature*, vol. 443, no. 7112, pp. 651–657, Oct. 2006, doi: 10.1038/nature05185.

A. O. Eketunde, “Diabetes as a Risk Factor for Breast Cancer,” *Cureus*, May 2020, doi: 10.7759/cureus.8010.

E. Ferraro, J. Z. Drago, and S. Modi, “Implementing antibody-drug conjugates (ADCs) in HER2-positive breast cancer: state of the art and future directions,” *Breast Cancer Res.*, vol. 23, no. 1, Dec. 2021, doi: 10.1186/s13058-021-01459-y.

S. Galbreath and T. Goswami, “Biomechanical Behavior of Female Breast—A Review,” *BioMed*, vol. 5, no. 1, p. 5, Jan. 2025, doi: 10.3390/biomed5010005.

A. Gefen and B. Dilmoney, “Mechanics of the normal woman’s breast,” *Technol. Health Care*, vol. 15, no. 4, pp. 259–271, July 2007, doi: 10.3233/THC-2007-15404.

E. Geuna, G. Curigliano, and F. Montemurro, “De-escalation in low-risk, HER2-positive breast cancer,” *Lancet Oncol.*, vol. 24, no. 3, pp. 200–201, Mar. 2023, doi: 10.1016/s1470-2045(23)00064-5.

L. Gozzelino, M. C. De Santis, F. Gulluni, E. Hirsch, and M. Martini, “PI(3,4)P2 Signaling in Cancer and Metabolism,” *Front. Oncol.*, vol. 10, Mar. 2020, doi: 10.3389/fonc.2020.00360.

B. Han, X. Lin, and H. Hu, “Regulation of PI3K signaling in cancer metabolism and PI3K-targeting therapy,” *Transl. Breast Cancer Res.*, vol. 5, pp. 33–33, Oct. 2024, doi: 10.21037/tbcr-24-29.

X. Hou *et al.*, “Phosphoinositide signaling at the cytoskeleton in the regulation of cell dynamics,” *Cell Death Dis.*, vol. 16, no. 1, Apr. 2025, doi: 10.1038/s41419-025-07616-x.

L. A. Huppert, O. Gumusay, D. Idossa, and H. S. Rugo, “Systemic therapy for hormone receptor-positive/human epidermal growth factor receptor 2-negative early stage and metastatic breast cancer,” *CA. Cancer J. Clin.*, vol. 73, no. 5, pp. 480–515, Sept. 2023, doi: 10.3322/caac.21777.

P. A. Janmey, R. Bucki, and R. Radhakrishnan, “Regulation of actin assembly by PI(4,5)P2 and other inositol phospholipids: An update on possible mechanisms,” *Biochem. Biophys. Res. Commun.*, vol. 506, no. 2, pp. 307–314, Nov. 2018, doi: 10.1016/j.bbrc.2018.07.155.

K. A. Kjærgaard *et al.*, “Risk of type 2 diabetes after breast cancer treatment: a population-based cohort study in Denmark,” *JNCI J. Natl. Cancer Inst.*, vol. 117, no. 3, pp. 537–544, Mar. 2025, doi: 10.1093/jnci/djae261.

H. Li, L. Prever, E. Hirsch, and F. Gulluni, “Targeting PI3K/AKT/mTOR Signaling Pathway in Breast Cancer,” *Cancers*, vol. 13, no. 14, p. 3517, July 2021, doi: 10.3390/cancers13143517.

C. Lin *et al.*, “Efficacy of platinum-based and non-platinum-based drugs on triple-negative breast cancer: meta-analysis,” *Eur. J. Med. Res.*, vol. 27, no. 1, Oct. 2022, doi: 10.1186/s40001-022-00839-0.

J. Lin *et al.*, “The roles of glucose metabolic reprogramming in chemo- and radio-resistance,” *J. Exp. Clin. Cancer Res.*, vol. 38, no. 1, Dec. 2019, doi: 10.1186/s13046-019-1214-z.

S. Matou-Nasri, M. Aldawood, F. Alanazi, and A. L. Khan, “Updates on Triple-Negative Breast Cancer in Type 2 Diabetes Mellitus Patients: From Risk Factors to Diagnosis, Biomarkers and Therapy,” *Diagnostics*, vol. 13, no. 14, p. 2390, July 2023, doi: 10.3390/diagnostics13142390.

L. Morrison, S. Loibl, and N. C. Turner, “The CDK4/6 inhibitor revolution — a game-changing era for breast cancer treatment,” *Nat. Rev. Clin. Oncol.*, vol. 21, no. 2, pp. 89–105, Feb. 2024, doi: 10.1038/s41571-023-00840-4.

A. Morrot *et al.*, “Metabolic Symbiosis and Immunomodulation: How Tumor Cell-Derived Lactate May Disturb Innate and Adaptive Immune Responses,” *Front. Oncol.*, vol. 8, Mar. 2018, doi: 10.3389/fonc.2018.00081.

A. Mujalli *et al.*, “Exploring the Role of PI3P in Platelets: Insights from a Novel External PI3P Pool,” *Biomolecules*, vol. 13, no. 4, p. 583, Mar. 2023, doi: 10.3390/biom13040583.

E. I. Obeagu and G. U. Obeagu, “Breast cancer: A review of risk factors and diagnosis,” *Medicine (Baltimore)*, vol. 103, no. 3, p. e36905, Jan. 2024, doi: 10.1097/md.0000000000036905.

K. Page *et al.*, “Next Generation Sequencing of Circulating Cell-Free DNA for Evaluating Mutations and Gene Amplification in Metastatic Breast Cancer,” *Clin. Chem.*, vol. 63, no. 2, pp. 532–541, Feb. 2017, doi: 10.1373/clinchem.2016.261834.

C. Porta, C. Paglino, and A. Mosca, “Targeting PI3K/Akt/mTOR Signaling in Cancer,” *Front. Oncol.*, vol. 4, Apr. 2014, doi: 10.3389/fonc.2014.00064.

Y. Posor, W. Jang, and V. Haucke, “Phosphoinositides as membrane organizers,” *Nat. Rev. Mol. Cell Biol.*, vol. 23, no. 12, pp. 797–816, Dec. 2022, doi: 10.1038/s41580-022-00490-x.

M. Prvanović *et al.*, “Role of PTEN, PI3K, and mTOR in Triple-Negative Breast Cancer,” *Life*, vol. 11, no. 11, p. 1247, Nov. 2021, doi: 10.3390/life11111247.

P. Ramteke, A. Deb, V. Shepal, and M. K. Bhat, “Hyperglycemia Associated Metabolic and Molecular Alterations in Cancer Risk, Progression, Treatment, and Mortality,” *Cancers*, vol. 11, no. 9, p. 1402, Sept. 2019, doi: 10.3390/cancers11091402.

A. Sánchez López de Nava and A. Raja, “Physiology, Metabolism,” in *StatPearls*, Treasure Island (FL): StatPearls Publishing, 2025. Accessed: July 17, 2025. [Online]. Available: http://www.ncbi.nlm.nih.gov/books/NBK546690/

T. Sella *et al.*, “Neoadjuvant Endocrine Therapy in Clinical Practice: A Review,” *JAMA Oncol.*, vol. 7, no. 11, p. 1700, Nov. 2021, doi: 10.1001/jamaoncol.2021.2132.

S. Shao *et al.*, “Diabetes and Overall Survival among Breast Cancer Patients in the U.S. Military Health System,” *Cancer Epidemiol. Biomarkers Prev.*, vol. 27, no. 1, pp. 50–57, Jan. 2018, doi: 10.1158/1055-9965.epi-17-0439.

P. Sharma *et al.*, “Clinical and Biomarker Results from Phase I/II Study of PI3K Inhibitor Alpelisib plus Nab-paclitaxel in HER2-Negative Metastatic Breast Cancer,” *Clin. Cancer Res.*, vol. 27, no. 14, pp. 3896–3904, July 2021, doi: 10.1158/1078-0432.ccr-20-4879.

M. Shastry, S. Jacob, H. S. Rugo, and E. Hamilton, “Antibody-drug conjugates targeting TROP-2: Clinical development in metastatic breast cancer,” *The Breast*, vol. 66, pp. 169–177, Dec. 2022, doi: 10.1016/j.breast.2022.10.007.

R. L. Siegel, T. B. Kratzer, A. N. Giaquinto, H. Sung, and A. Jemal, “Cancer statistics, 2025,” *CA. Cancer J. Clin.*, vol. 75, no. 1, pp. 10–45, Jan. 2025, doi: 10.3322/caac.21871.

A. Stincone *et al.*, “The return of metabolism: biochemistry and physiology of the pentose phosphate pathway,” *Biol. Rev.*, vol. 90, no. 3, pp. 927–963, Aug. 2015, doi: 10.1111/brv.12140.

X. Sun *et al.*, “Association between diabetes status and breast cancer in US adults: findings from the US National Health and Nutrition Examination Survey,” *Front. Endocrinol.*, vol. 14, p. 1059303, June 2023, doi: 10.3389/fendo.2023.1059303.

T. TeSlaa, M. Ralser, J. Fan, and J. D. Rabinowitz, “The pentose phosphate pathway in health and disease,” *Nat. Metab.*, vol. 5, no. 8, pp. 1275–1289, Aug. 2023, doi: 10.1038/s42255-023-00863-2.

S. Thomsen and D. Tatman, “Physiological and Pathological Factors of Human Breast Disease That Can Influence Optical Diagnosis[a],” *Ann. N. Y. Acad. Sci.*, vol. 838, no. 1, pp. 171–193, Feb. 1998, doi: 10.1111/j.1749-6632.1998.tb08197.x.

H. Villanueva *et al.*, “The Emerging Roles of Steroid Hormone Receptors in Ductal Carcinoma in Situ (DCIS) of the Breast,” *J. Mammary Gland Biol. Neoplasia*, vol. 23, no. 4, pp. 237–248, Dec. 2018, doi: 10.1007/s10911-018-9416-0.

J. Wang *et al.*, “Progression from ductal carcinoma in situ to invasive breast cancer: molecular features and clinical significance,” *Signal Transduct. Target. Ther.*, vol. 9, no. 1, Apr. 2024, doi: 10.1038/s41392-024-01779-3.

A. Wodarz and I. Näthke, “Cell polarity in development and cancer,” *Nat. Cell Biol.*, vol. 9, no. 9, pp. 1016–1024, Sept. 2007, doi: 10.1038/ncb433.

X. Xiong *et al.*, “Breast cancer: pathogenesis and treatments,” *Signal Transduct. Target. Ther.*, vol. 10, no. 1, Feb. 2025, doi: 10.1038/s41392-024-02108-4.

A. Yoneda *et al.*, “Phosphatidylinositol 4,5-bisphosphate is localized in the plasma membrane outer leaflet and regulates cell adhesion and motility,” *Biochem. Biophys. Res. Commun.*, vol. 527, no. 4, pp. 1050–1056, July 2020, doi: 10.1016/j.bbrc.2020.05.040.

Curriculum Vitae

Aaron Kile

822 Hildebrand Dr • Indianapolis, IN 46217 • Aakile@iu.edu • 3174863698

ORCID: 0009-0008-5701-4098

Education

Indiana University

Indianapolis

Biochemistry & Molecular Biology, Cancer Focus. GPA: 3.91

08/24 – 010/25
Thesis: Towards Targeted Detection of Triple Negative Breast Cancer and its Metastasis

Indiana University

Indianapolis

Neuroscience Major. GPA: 3.5

08/20 – 05/24
Chemistry & Africana Studies Minors

Perry Meridian High School

Indianapolis

Academic Honors. GPA: 3.8
01/17 – 05/20

Capstone: Efficiency of Perception in both simple and complex images among people of different genders, ages, ethnicities and vision types.

Experience

IUSM

Indianapolis, IN

Graduate Student
08/24 – 09/25

- Engaging with field specific experts on biochemical topics.
- Collaborating with a faculty member in Biochemistry to work and write a thesis.
- Networking with interdepartmental and interinstitutional faculty to execute projects on my thesis.
- Managing time to be efficient in both class work and laboratory work.

Indianapolis Motor Speedway
Indianapolis, IN

Emergency Medical Technician
09/22 – 05/24

- Worked with a full medical team to provide medical car to drivers and spectators.
- Demonstrated composure in stressful medical emergencies.
- Gave instruction and direction to team members to best serve patients.
- Controlled chaotic scenes to offer best care to patients.

Morgan County EMS
Indianapolis, IN

Emergency Medical Technician
09/22 – 05/24

- Managed critical patients for long commutes to the hospital.
- Assisted paramedics to care for a diverse group of patient cases.
- Responded with alertness to medical calls for 24 hour shifts often.
- Followed a written set of protocols outlining best medical practices.

Kimble-Hill Lab
Indianapolis, IN

Research Technician
09/22 – 05/24

- Performed a variety of experimental assay to test hypotheses.
- Mentored two junior students in the lab.
- Prepared and presented results at more than 10 local and national conferences.
- Collaborated with other students to manage multiple tasks and projects.

1619 Project
Indianapolis, IN

Undergraduate Researcher
08/22 – 08/22

- Mastered VR gaming software to create a basic prototype for the project.
- Employed creative skills within the scope of the literature to create a VR prototype.
- Engaged with a team to execute dynamic weekly goals.
- Presented the progress of the work at local conferences.

Baucum Lab
Indianapolis, IN

Undergraduate Researcher
02/21 – 07/21

- Worked with graduate students to cultivate good laboratory skills.
- Developed insight into reading scientific papers.
- Applied in-class knowledge to real world scientific questions.
- Sharpened critical thinking skills in combination with hands on skills.

Amazon
Indianapolis, IN

Returns Associate
06/20 – 08/20

- Handled a variety of customer returns to ensure a smooth customer experience.
- Screened returned items for potential hazards and damage.
- Navigated COVID-19 precautions in a large, populated warehouse.
- Managed a nightshift schedule without diminished output.

Walmart
Indianapolis, IN

Front End Cashier
02/19 – 07/20

- Facilitated the checkout experience for customers.
- Organized the checkout aisle to assist marketing efforts.
- Engaged in short conversations with customers to further impress a good experience.
- Assisted managers in answering customer questions about various products.

JCPenney
Indianapolis, IN

Sales Associate
10/18 – 03/20

- Sought and assisted customers for find what they needed.
- Suggested items to customers to drive sales for the company.
- Persuaded customers to join the rewards program for ensure their return.
- Placed online orders for customers to avoid losing instore sales.

McDonalds
Indianapolis, IN

Team Member
09/17 – 10/18

- Managed inventory fulfillment.
- Supervised a team to shelve and restock inventory.
- Spearheaded the disassembly, cleaning, and reassembly of dairy machines.
- Trained new team members various tasks in the store.

Leadership & Activities

IU Olaniyan Scholars Program
Indianapolis, IN

Undergraduate Mentor
08/24 – Present

- Inspiring students to overcome challenges and be well rounded scholars.
- Engaging students in academic and community research projects.

IU Engaged Learning
Indianapolis, IN

Student Highlight Story
05/2024

- Published article covering my undergraduate research journey and impact here.
- Short video narrating these research opportunities here.

LifePoint Church
Indianapolis, IN

Middle School Student Leader
08/21 – 05/24

- Facilitated discussion groups about bible stories for students.
- Challenged students to apply critical thinking and empathy in all areas of their lives.

CRU- International Student Organization
Indianapolis, IN

Board Member
08/23 – 05/24

- Collaborated with other board members to inform the organization's direction at IU Indianapolis.
- Created a welcoming and safe environment for new students.

CRU- International Student Organization
Chicago, IL

Summer Student Director
06/22 – 08/22

- Oversaw projects of students from different universities in the Midwest.
- Led leadership meetings with other leaders.

CRU- International Student Organization
Indianapolis, IN

Men's Bible Study Leader
08/21 – 05/24

- Organized and prepared Bible study sessions with college students of diverse backgrounds.
- Fostered group cohesion through creative group activities and games.

Lollapalooza
Chicago, IL

EMT Volunteer
07/22

- Screened crowds for people who needed medical attention.
- Worked with trained medical personnel to provide medical care to fans at the concert.

IU Experiential & Applied Learning
Indianapolis, IN

Project Team Leader
01/22 – 05/22

- Facilitated team dynamics to foster a productive working experience for all people.
- Oversaw our team as we created a deliverable to our client found here.

Kimble-Lab
Indianapolis, IN

Student Mentor
05/23 – 05/24

- Explained and provided clarity ongoing projects to junior students in the lab.
- Gave oversight to newer students as they carried out various tasks.

LifePoint Church
Indianapolis, IN

Friendship Life Group Leader
11/20 – 04/22

- Fostered healthy working relationships with adults with special needs.
- Assisted adults with various special needs to learn different social emotional regulation skills.

Perry Meridian High School
Indianapolis, IN

Best Buddies
08/19 – 03/20

- Assisted special needs students to have a comprehensive experience.
- Programmed some after-school activities for the students to improve relationships.

Night to Shine- Tim Tebow Foundation
Indianapolis, IN

Prom Chaperon
07/19

- Helped promote a normal prom experience to Special needs high school students.
- Created and monitored the space to keep the prom experience safe and fun for all students.

Perry Meridian High School
Indianapolis, IN

Fellowship for Christian Athletes (FCA)
08/18 – 05/20

- Organized weekly gathering for participating students.
- Spearheaded initiatives to reach more students in the high school.

Awards

University Fellowship
Competitive award given to the best MA/MS and PhD students entering Indianapolis' research based graduate programs each fall (2024).

IU Cancer Center Award
IU Melvin and Bren Simon Comprehensive Cancer Center Research Conference 2023: Best Poster in Basic Science, Behavioral, Population science/ Epidemiology and Translational/ Clinical Research.

IU Melvin and Bren Simon Comprehensive Cancer Center Research Conference 2023: Best Poster in Community Engagement Research.

IUURC Award
Second place in oral presentation competition (2021)

Dean's List
For achieving above a 3.5 in each semester (12/2020, 12/2021, 05/2022, 05/2023, 12/2024, 05/2024)

Jaguar Excellence Award
Matriculating and maintaining a cumulative GPA of 3.0 (2020 – 2024)

Indianapolis Professional Association
Achievement Award (2020)

National Honors Society
Outstanding academic achievement and commitment to service (2019 – 2020)

Attended Conferences

Peachy Amelia Conference: 2022 - 2025
ABRCMS: 2024
IU Cancer Center Research Day: 2023**,** 2024
IUI Research Day: 2022 - 2024
Metabolism Conference: 2023
ACS Indianapolis: 2023
CRL Research Conference: 2021 - 2024
CRL Summer Symposium: 2021- 2024

Olaniyan Research Day: 2020 - 2024

Skills

Languages: English, Swahili, Luganda.

Communication: Presentations, Electronic messaging, etc.

Computer Skills: Microsoft Office 365, Image J, FIJI, Unreal Engine, Photoshop, Adobe, Zoom etc.

Lab Skills: Cell Culture, Spot Blot, Transfection, lentiviral Infection, DNA Electrophoresis, Following a protocol etc.

Leadership: Mentoring, Academic, Non-profit, etc.

Networking: Formal and informal conversations and settings